
DOMAIN GENERALISATION FOR OBJECT DETECTION UNDER COVARIATE AND CONCEPT SHIFT

Karthik Seemakurthy
Lincoln Institute of Agri-Food Technology
University of Lincoln
Lincoln, UK
kseemakurthy@lincoln.ac.uk

Erchan Aptoula
Faculty of Engineering and Natural Sciences (VPALAB)
Sabanci University
Istanbul, Türkiye
erchan.aptoula@sabanciuniv.edu

Charles Fox, Petra Bosilj
School of Computer Science
University of Lincoln
Lincoln, UK
{chfox, pbosilj}@lincoln.ac.uk

ABSTRACT

Domain generalisation aims to promote the learning of domain-invariant features while suppressing domain-specific features, so that a model can generalise better to previously unseen target domains. An approach to domain generalisation for object detection is proposed, the first such approach applicable to any object detection architecture. Based on a rigorous mathematical analysis, we extend approaches based on feature alignment with a novel component for performing class conditional alignment at the instance level, in addition to aligning the marginal feature distributions across domains at the image level. This allows us to fully address both components of domain shift, i.e. covariate and concept shift, and learn a domain agnostic feature representation. We perform extensive evaluation with both one-stage (FCOS, YOLOv3) and two-stage (Faster R-CNN) detectors, on a newly proposed benchmark comprising several different datasets for autonomous driving applications (Cityscapes, BDD10K, ACDC, IDD) as well as the GWHD dataset for precision agriculture, and show consistent improvements to the generalisation and localisation performance over baselines and state-of-the-art.

Keywords Domain Generalisation · Object Detection · Domain Shift

1 Introduction

Object detection (OD) is the task of identifying and localising all instances of a certain type (or types) of object in an image. Benchmark performances have increased significantly using deep learning approaches [1, 2, 3, 4, 5, 6, 7, 8]. However, deploying these vision models in autonomous systems continues to be challenging, as factors such as viewpoint, background, weather, and capture devices compound with the variations in object appearance. The resulting distribution discrepancy between training and testing data is called *domain shift* and degrades model performance at deployment [9, 10]. Fig. 1 shows examples illustrating the domain shift that can be encountered in autonomous farming and driving contexts. One can observe significant levels of variations across the appearance of wheat and vehicles in terms of size, shape, illumination, and their positioning in the scene, made more challenging by changing weather conditions.

Alleviating the impact of domain shift by increasing the amount and diversity of annotated training data is both expensive and time consuming, and still provides no guarantee that all deployment scenarios will be adequately represented. In practice, training data obtained from the specific deployment (target) domain is often sparse or unavailable. Therefore, *domain generalisation* (DG) addresses the domain shift by dividing the training data into several known domains during

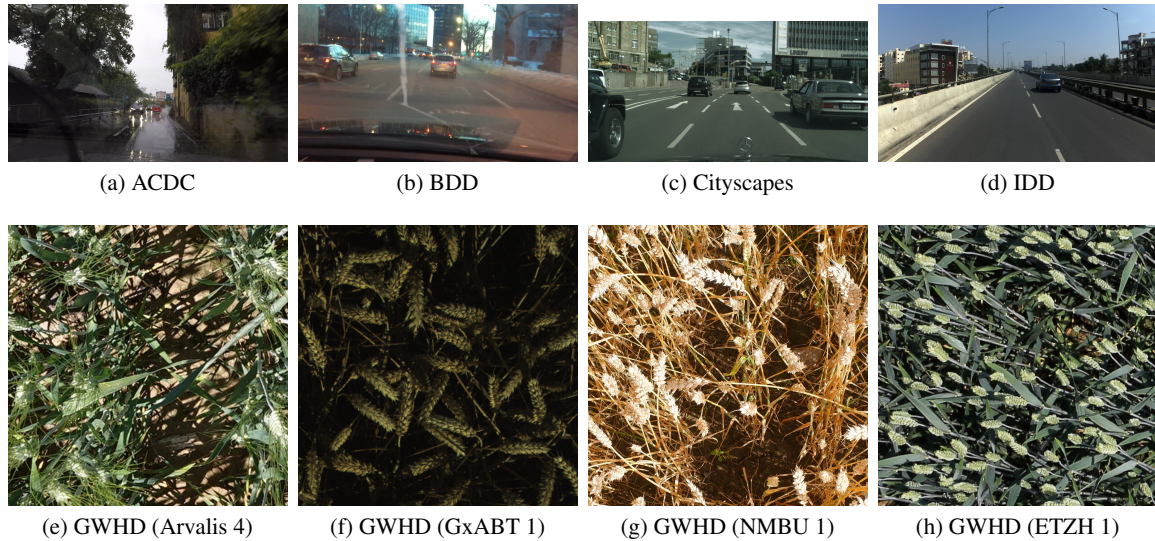


Figure 1: Samples from various datasets used in our experiments.

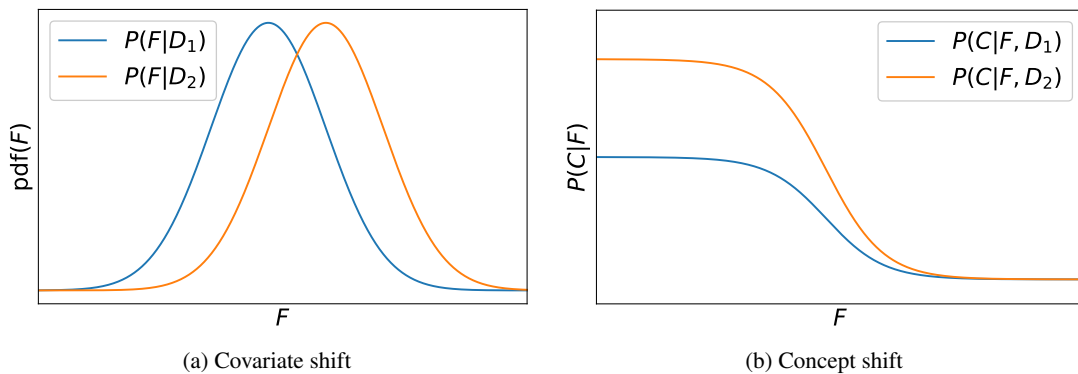


Figure 2: Different types of domain shift which can describe the relationship between two domains D_1 and D_2 , on a simplified example of using a single feature F to predict the existence of a class C . Covariate shift, shown in (a), describes the situation when the feature (input data) distribution changes between domain. Concept shift, shown in (b) describes the situation where the relationship between the class C and the features F changes. The overall distribution shift between two domains is typically a combination of covariate and concept shift.

training to learn how to suppress domain-specific information. The goal is to directly learn a single, unchanging set of parameters which are able to perform well on previously unseen domains. However, recent surveys on the topic of DG [11, 12] indicate the lack of a systematic analysis of DG for OD. In this paper, we offer a rigorous mathematical treatment of feature alignment approaches in OD while addressing both components of domain shift, namely covariate and concept shift (Fig. 2, Eq. (1)). Covariate shift describes the change in the input distribution, while concept shift refers to the change in the relationship between the predictive features and the expected output [13]. Note that there is an alternative model of domain shift, briefly shown later in Eq. (2), decomposing it into label and manifestation shifts, which we do not use in this paper. We show that aligning the marginal feature distributions across domains at the image level [14], and even the instance level [15] only addresses the covariate shift, which is necessary, but not sufficient to promote DG in OD. We further show that addressing concept shift by aligning class conditional distributions at the instance level, as well as ensuring consistency between instance and image level features [16, 17] consistently improves DG for OD. This paper brings together and builds upon the previous work by the authors [16, 17] to show how our proposal to jointly address both the covariate and concept components of domain shift can be applied to any object detection architecture, the first architecture-agnostic DG-OD approach. We include an extensive evaluation of

our approach on both one-stage (YOLOv3, FCOS) and two-stage (Faster R-CNN) object detection architectures, 4 autonomous driving datasets and 1 autonomous farming dataset, improving the performance of all baseline architectures and outperforming the state-of-the-art approaches [14, 18] approaches on their own benchmarks. Finally, we propose an extended and improved benchmark for DG in OD for autonomous driving, relying on 4 distinct and independent datasets (compared to the one used by [18], which only uses 3 datasets, one of which is synthetically derived from another). Our implementations and models are made available to encourage further research on this topic¹.

2 Related Work

This section begins by explaining the challenges encountered in the object detection task during test-time, caused by domain shift. Then, it discusses different causes of domain shift and ways of addressing it, depending on the amount and type of available training data and annotations. Families of approaches to domain generalisation are explained with applications to classification, as the majority of works addressing DG directly still focus primarily on the classification task. Finally, the applications of DG to tasks which distinguish between image and object-level features are discussed, with a special focus on the only three published works addressing domain generalisation for the object detection task [14, 18, 19].

Object detection. Classical approaches to OD relied on handcrafted features and formulated OD as a sliding window classification problem [20, 21, 22], combining classification and localisation in a single task. The empirical success of deep neural networks (DNNs) – which automatically extract high performing features – [23, 24] has resulted in their widespread adoption. Most CNN-based approaches to object detection can be categorised as either single-stage [1, 2, 3, 25, 26, 27, 28, 29, 30, 31] or two-stage [4, 5, 6, 32, 33], but OD can still be interpreted as a combination of a classification and localisation task. *Two-stage* approaches developed from the Region-based CNN (R-CNN) family [4, 32, 33] are characterised by a network trained to classify region proposals selected from the image in a separate preceding localisation step. *Single-stage* approaches perform localisation and classification simultaneously and have only recently reached the performance of two-stage approaches [1]. However, all of these architectures and a number of follow-up works [3, 5, 6] operate under the assumption that the testing data originates from the same domain and distribution as the training data and their performance consequently degrades on out-of-domain (OOD) data. When addressing domain shift, it is important to note that different to classification, where instance and image features are one and the same, in OD image level domain features can have a substantially different distribution to instance level class features. Therefore, our treatment of domain shift for OD addresses shift jointly at the image and instance level.

Domain shift. A number of techniques exist to directly or indirectly address domain shift. Transfer learning (TL) [34] is one of the best-known examples, enabled by a high transferability of pre-trained deep features, especially from the lower layers. Architectures pre-trained on a large corpus such as ImageNet [35] are fine-tuned for a different but related task. Contrary to DG, TL requires annotated data from the target domain, but can decrease both the amount of time and annotations needed by several orders of magnitude compared to training from scratch. The shift comes both from the distribution change between source and target domains, and a disjoint label space. It has been noted that the effectiveness of TL drops with increasing domain shift [36, 37, 38, 39]. *One-shot* and *few-shot learning* (OSL and FSL) [40] are a special case of transfer learning, where the representation of a new class is learned only from a single (or a handful of) labelled image(s) of that class. Unlike TL and OSL/FSL approaches which require fully annotated target domain data, *self-supervised learning* (SSL) [41] approaches leverage unlabelled data to minimise the shift in feature space. This can be realised either sequentially, as a pre-training step followed by a classical supervised TL [42, 43], or in a semi-supervised multi-task learning setup, where the unlabelled data is used in conjunction with a (typically much smaller quantity of) labelled data [44, 45, 46]. Since the secondary task, relying on unlabelled data, has a regularising effect on the learned features [47], this paradigm has also been applied for DG [48]. *Domain randomisation* [49, 50] is a complementary approach to DG, which relies on synthetically generated variations of the input data to obtain more generalisable features. *Domain adaptation* (DA) [15, 51] the closest topic to DG, as they both aim to address the domain shift encountered in new environments (target domain distribution shift) without the change to the label space. However, unlike DG, where no information about the target data distribution is known, DA relies on sparsely labelled or unlabelled target domain data (or other information providing insight into target data distribution) during training.

Domain generalisation in classification. DG was first studied by Blanchard et al. [52] in the context of medical imaging, while the terminology was introduced later by Muandet et al. [53]. Earlier studies have explored fixed shallow features [53, 54, 55, 56, 57], while more recent investigations design architectures to address domain shift [58] or learning algorithms to optimise standard architectures [59, 60, 61]. One of the most common approaches to DG (as well as DA) is *feature alignment* [53, 62, 63], where the aim is to minimise the difference between the features representations of the source domains in order to learn a domain-invariant representation. Typical alignment techniques

¹Final github repo will be shared upon acceptance

include domain-adversarial learning [63], moments [64], contrastive loss [65], KL-divergence [66] and maximum mean discrepancy [67]. Contrary to feature alignment which attempts to make the whole model domain-invariant, in approaches based on *representation disentanglement* [58, 68], the models contain both domain-specific and domain-agnostic parts. In *meta-learning*, training data is split into meta-train and meta-test sets which exhibit domain shift akin to the one expected at test-time, with the goal of learning how to train using the meta-train set in a way that improves the performance on the meta-test set. MAML [69], a meta-learning technique for DA, has been repurposed for DG [59], and extended in numerous follow-up works [70, 71]. Approaches performing advanced *data augmentations* attempt to diversify the training data, e.g. by applying off-the-shelf style transfer models [72] or learning to synthesise new domains [73]. For a more detailed review of different domain generalisation approaches, we refer the reader to a review paper by Zhou et al. [11].

Domain generalisation beyond classification. Despite the numerous advances in understanding and addressing domain shift, there are not many works dealing with DG, or domain shift at all, in tasks beyond classification. A DG approach based on meta-learning was proposed for semantic segmentation [59], however, different to the typical DG setting, this approach requires additionally processing the target domain data at inference time. DG has also been applied to person re-identification [74] and face presentation [75, 76], however both of these applications have a key characteristic in common with classification, namely the fact that the image-level and object-level features are one and the same. Chen et al. [15] propose a DA approach for minimising the domain shift in OD, a task which distinguishes between image and instance-level features. Their approach is based on feature alignment, and attempts to perform feature alignment consistently between the image and instance-level features, similar to our proposal. However, while it can be applied to DG with minimal modifications, it relies on the assumption that the class distribution and classifier behaviour is consistent across domains. This assumption has been shown to be false, especially when the shift between input image domains is significant [63, 67, 77, 78, 79, 80], which has been addressed by this work, using a similar approach to that which Zhao et al. [77] applied to classification. DG for OD has been explicitly addressed only by Liu et al. [14] (which was extended by Chen et al. [19]) and Lin et al. [18]. In common with the work proposed herein, Liu et al. [14] also rely on feature alignment to achieve DG, however, unlike our work, they only address covariate shift by aligning the image-level features, similarly to classification approaches. In addition, they rely on style transfer to generate new domain examples, and implement the feature alignment jointly through the Gradient Reversal Layer (GRL)[62] (like us) and Invariant Risk Minimisation (IRM) [81] (which we do not do). The follow-up work to Liu et al. [14], proposed by Chen et al. [19], improves the new domain synthesis, and implements feature alignment through contrastive learning, however still only addresses the covariate shift at the image level. Like our own work, the approach for Lin et al. [18] is tailored specifically for OD, addressing domain shift both at the image and instance level. However, it conflates two incompatible domain shift models (Eqs. 1 and 2) by attempting to address covariate and label shift at the same time. Finally, while all of these DG for OD approaches are tailored for one specific architecture (Liu et al. [14], Chen et al. [19] work on YOLOv3 [25], while Lin et al. [18] work with Faster R-CNN [4]), the work presented in this paper constitutes the first DG for OD approach which can be used with any detector.

3 Preliminaries

In this section the DG task is formally defined, and the mathematical context used by the proposed solution is presented.

Let a *model* be any function which takes an image as input, and transforms it into a feature vector according to its parameters, and returns a set of bounding boxes and a vector of class probabilities for each bounding box, based only on these features and additional parameters. Let a *trainer* be any system which takes images, ground truth bounding boxes containing objects of interest as well as their respective classes as training data, a model, and a loss function quantifying the system’s performance in terms of classification accuracy and bounding box prediction quality, all as input; and returns a set of model parameters which minimises the loss function between the model outputs and the training data, called a *trained model*.

DG assumes that the training data is generated from multiple domains, and labelled with these domains in addition to the bounding boxes and classes. A *DG trainer* is a system which takes similar inputs to a trainer with these domain labels added to images, and returns a trained model capable of generalising to unseen target domains without compromising the classification or bounding box prediction performance.

Let $\mathbf{I} \times \mathbf{C} \times \mathbf{B} \times \mathbf{D}$ be the sample space under observation. Here $I \in \mathbf{I}$ is an image, and $B \in \mathbf{B} = \mathbb{R}^4$ is a bounding box as a tuple (x, y, w, h) , of its central coordinate, width and height. $C \in \mathbf{C}$ denotes the detection class. $D \in \mathbf{D}$ is the domain to which an image belongs, $|\mathbf{C}|$ is the total number of classes in the training data, $|\mathbf{D}|$ is the total number of domains in the training data, and $|D|$ is the number of images in domain D .

Let $P(I, C, B|D)$ be the ground truth joint distributions defined on $\mathbf{I} \times \mathbf{C} \times \mathbf{B}$ given domain D . The DG trainer’s task is to take as input a model and ground truth data from $\mathbf{I} \times \mathbf{C} \times \mathbf{B} \times \mathbf{D}$, and return a trained model capable of domain invariant detection.

Let a model be defined by the tuple $(f, c, b, \phi, \gamma, \beta)$ of functions and parameters for a feature vector extractor $F = f(I; \phi)$, a classifier on these features, $c(F; \gamma) \approx P(C|I)$, and a bounding box predictor $b(F; \beta) \approx P(B|I)$, respectively. Let $Q(C, B|I)$ be the joint distribution induced by a model given an image. The DG trainer’s task is to optimise the parameters in order to best approximate $Q(C, B|I) \approx P(C, B|I)$. Note that this equation is independent of domain D .

Notation conventions: Q is parameterised by – and so depends on – all of the parameters, but we omit them in the notation for brevity unless specified otherwise. All distributions involving F are also parameterized by ϕ which we also omit from notation for the sake of brevity. Expectations, entropies, and other functionals are assumed to be taken over the conditioned, not conditioning variables unless otherwise stated, for example $\langle P(A, B|C, D) \rangle$ abbreviates $\langle P(A, B|C, D) \rangle_{A, B}$ (the expectation values of A and B given particular C and D).

To approximate the domain specific joint distributions $P(F, C, B|D)$ with a common $Q(F, C, B)$, we need to approximate all of the domain specific conditionals $P(C, B|F, D)$ with a common conditional $Q(C, B|F)$ and the domain specific marginals $P(F|D)$ by a common marginal $Q(F)$,

$$P(F, C, B|D) = P(C, B|F, D)P(F|D) \approx Q(C, B|F)Q(F). \quad (1)$$

Many state-of-the-art studies [15, 53] attribute domain shift exclusively to the difference in marginals $P(F|D) \neq P(F|D')$ (i.e. to covariate shift, Fig. 2a), while assuming conditionals to be stable across domains, $P(C, B|F, D) = P(C, B|F, D')$ (i.e. no concept shift, Fig. 2b).

Alternatively, domain shift $P(F, C, B|D)$ can also be decomposed as:

$$P(F, C, B|D) = P(F|C, B, D)P(C, B|D), \quad (2)$$

where changes between different domains in $P(C, B|D)$ are called *label shift*, and in $P(F|C, B, D)$ are referred to as *manifestation shift*. It is worth noting that the two domain shift models in Eqs. (1) and (2) are mutually exclusive, as they rely on different assumptions about the causal direction between the class and the features in the real world.

The standard approach adopted by [15, 82] of finding ϕ to address covariate shift by equalising the marginals across domains is through an explicit feature-level domain discriminator $s(F; \psi) \approx P(D|F)$, by min-maxing the domain adversarial loss \mathcal{L}_{dadv} :

$$\min_{\phi} \max_{\psi} \mathcal{L}_{dadv}(\phi, \psi), \quad (3)$$

where \mathcal{L}_{dadv} is defined as [83]:

$$\mathcal{L}_{dadv}(\phi, \psi) = \sum_I \mathbf{1}_{D(I)} \cdot \log(s(f(I; \phi); \psi)), \quad (4)$$

where I ranges over the images in the training data, and $\mathbf{1}_D$ is the one-hot vector encoding the domain D of image I . This minmax game enables $F = f(I; \phi)$ to learn features whose domain cannot be distinguished by any $s(F; \psi)$, leading to equality of domain marginals,

$$\begin{aligned} P(F|D) &= P(F|D'), \quad \forall D, D' \\ &= Q(F) \end{aligned} \quad (5)$$

However, as pointed out by recent studies [63, 77, 78, 79], the stability of conditionals across domains cannot be guaranteed. Any method with the goal of achieving domain invariance needs to compensate for the variation in conditionals $P(C, B|F, D)$. In other words, the domain discriminator $s(F; \psi)$ creates invariance on the sample space $\mathbf{I} \times \mathbf{D}$ but not on $\mathbf{I} \times \mathbf{C} \times \mathbf{B} \times \mathbf{D}$. Moreover, the techniques proposed in recent studies [63, 77] are intended for classification and cannot be directly used to achieve generalised object detection.

4 Proposed Method

We now describe how to approximate the domain-specific conditionals $P(C, B|F, D) = P(C, B|F, D')$ with a common $Q(C, B|F)$. In conjunction with Eq. (3) this will lead to a DG trainer.

To approximate the domain-specific conditional distribution $P(C, B|F, D)$ of each domain D with a common distribution $Q(C, B|F)$, we minimise,

$$\min_{\phi, \gamma, \beta} \sum_D KL [P(C, B|F, D) || Q(C, B|F)] \quad (6)$$

$$= \min_{\phi, \gamma, \beta} \sum_D KL [P(C|B, F, D) || Q(C|B, F)] + \min_{\phi, \gamma, \beta} \sum_D KL [P(B|F, D) || Q(B|F)] \quad (7)$$

where $Q(C|B, F)$ and $Q(B|F)$ denote respectively the distributions associated with the instance level classifier and the bounding box predictor. Through the minimisation of the two terms in Eq. (7), the overall system is encouraged to transform the input images into a feature space where the both domain-specific instance level classifier (first term) and the bounding box predictor (second term) will be domain invariant. This implies that the optimisation in Eq. (7) along with Eq. (3) will result in a domain generalised trained model.

4.1 Classifier term

The first term in Eq. (7) can be further written as:

$$\min_{\phi, \gamma, \beta} \sum_D \langle \log \frac{P(C|B, F, D)}{Q(C|B, F)} \rangle \quad (8)$$

$$= \min_{\phi, \gamma, \beta} \left(\sum_D \langle \log P(C|B, F, D) \rangle - \sum_D \langle \log Q(C|B, F) \rangle \right) \quad (9)$$

$$= \min_{\phi, \gamma, \beta} \left(\sum_D -H(C|B, F, D) + \mathcal{L}_{cls} \right) \quad (10)$$

The first term in Eq. (9) is the sum of $|D|$ conditional negentropies $-H(C|B, F, D)$ over domains D . The second term in Eq. (9) is known as the **classification loss** \mathcal{L}_{cls} . Note that many algorithms already exist for minimising \mathcal{L}_{cls} so can be used as components of algorithms for minimising the whole of Eq. (9).

However such algorithms also need to minimise the conditional negentropy term, which is equivalent to maximising the conditional entropy $H(C|B, F, D)$. As both minimisations involve the same parameters, iterative algorithms which act in parallel to minimise both terms may compete to pull the solution in opposite directions.

To see the effect of perfectly maximising the conditional entropy $H(C|B, F, D)$ alone in Eq. (9) (i.e. temporarily ignoring the competing objective \mathcal{L}_{cls}), we adapt the following theorem from [77] for object detection:

Theorem 1: Assuming all the object classes are equally likely, maximising $H(C|B, F, D)$ is equivalent to minimising the Jensen-Shannon divergence between the $|C|$ conditional distributions $P(B, F|C, D)$ across classes. The global optimum can be achieved if and only if:

$$P(B, F|C, D) = P(B, F|C', D), \quad \forall C, C' \quad (11)$$

Even though this assumption can fail under a class imbalance scenario, balance can still be enforced through batch based biased sampling.

Proof: We use the derivation provided in the supplementary material of [77] and adapt it to the object detection setting by including the bounding box predictions B . Recall the definition of information gain G between any two random variables L and M :

$$G(L, M) = H(L) - H(L|M) \quad (12)$$

Let L be a discrete random variable which can take the values in $\{1, \dots, |C|\}$, then the relation between KL and Jensen-Shannon (JS) divergence is given by [84]:

$$JS[P(M|L=1), P(M|L=2), \dots, P(M|L=|C|)] = \langle KL[P(M|C) || P(M)] \rangle_C \quad (13)$$

By using the definition in Eq. (12), the class conditional negentropy can be expressed as

$$-H(C|B, F, D) = G(F, C, B|D) - H(C|D) \quad (14)$$

The first term of Eq. (14) can be expanded as

$$\begin{aligned}
 G(F, C, B|D) &= H(F, B|D) - H(F, B|C, D) \\
 &= \frac{1}{|\mathbf{C}|} \sum_C \langle \log \frac{P(F, B|C, D)}{P(F, B, D)} \rangle \\
 &= \langle KL(P(F, B|C, D) || P(F, B, D)) \rangle_C
 \end{aligned} \tag{15}$$

From Eqs. (14) and (15), it can be deduced that minimising the domain specific class conditional negentropy $-H(C|B, F, D)$ is equivalent to minimising the KL-divergence between $P(F, B|C, D)$ and $P(F, B, D)$. (Note that $H(C|D)$ is a ground truth constant which does not depend on our model parameters, so cannot be optimised.)

By using Eq. (13), minimising the KL divergence in Eq. (15) is equivalent to minimising the following Jensen-Shannon divergence:

$$JS[P(F, B|C = 1, D), P(F, B|C = 2, D), \dots, P(F, B|C = |\mathbf{C}|, D)] \tag{16}$$

whose global minimum occurs under the condition of Eq. (11) \square .

Eq. (11) shows that the minimisation of class conditional negentropy alone results in domain specific instance level features which have no discriminative ability to assign the correct class label corresponding to the objects in the image I – making them completely useless for our actual goal of detection. However, recall that in reality we do not wish to minimise this term alone, but rather use its hypothetical solution to pull against some existing method for minimising \mathcal{L}_{cls} in Eq. (10).

One way to solve Eq. (11) is to use adversarial learning, inspired by the minmax game approach proposed in [77, 83, 85]. We here introduce $|\mathbf{D}|$ new classifiers, $c(F; \gamma_D)$, each parameterised by a different, domain-specific γ_D , and propose the following **domain specific adversarial** classification loss function \mathcal{L}_{erc} ,

$$\min_{\phi} \max_{\{\gamma_D\}} \mathcal{L}_{erc}(\phi, \gamma_D) \tag{17}$$

where

$$\mathcal{L}_{erc}(\phi, \{\gamma_D\}) = \sum_D \langle \log Q(C|B, F, D; \gamma_D) \rangle \tag{18}$$

and $Q(C|B, F, D; \gamma_D)$ is the Q distribution with γ_D replacing its usual γ .

4.2 Bounding box term

To optimise the second term in Eq. (7), we adopt a strategy previously used by Chen et al. [15] for DA. Minimising the KL divergence between the terms $P(B|F, D)$ and $Q(B|F)$ is equivalent to building a bounding box predictor independent of the domain label D . Using Bayes' theorem gives,

$$P(D|B, F)P(B|F) = P(B|F, D)P(D|F) \tag{19}$$

where $P(D|B, F)$ represents the instance level domain label predictor, $P(B|F, D)$ is the domain specific bounding box predictor, and $P(D|F)$ is the image level domain label predictor. From Eq. (19), we can observe that if there is a consistency between the image and instance level domain label predictor then the bounding box predictor will be invariant to domains, i.e. $P(B|D, F) = P(B|F)$.

The input $F[B]$ to the instance-level domain classifier will be the subset of image I features, computed at locations within the bounding box B by $f(I[B]; \phi)$. The **instance level domain classification loss** \mathcal{L}_{dins} employed at classifier $t(F[B]; \tau) \approx P(D|F[B])$ is:

$$\mathcal{L}_{dins}(\phi, \tau) = \sum_{B \sqsubset I} \langle \log(P(D|B, F)) \rangle = \sum_D \sum_{B \sqsubset I} \mathbf{1}_D \cdot \log(t(F[B]; \tau)) \tag{20}$$

where $B \sqsubset I$ ranges over the bounding boxes detected in image I . As shown in Eq. (19), in order to achieve invariant bounding box prediction across domains, we need a **consistency regularisation loss** \mathcal{L}_{cst} [15]:

$$\mathcal{L}_{cst}(\phi, \beta) = \|\langle t(F[B]; \tau) - s(F; \psi) \rangle_{B \sqsubset I} \|_2 \tag{21}$$

which is the ℓ^2 -norm of the average difference between instance and image domain discriminator vectors. Consequently, the main loss function that is to be used for training the system is given by:

$$\begin{aligned} \min_{\phi, \gamma} \max_{\psi, \{\gamma_D\}, \tau} \mathcal{L}(\phi, \gamma, \psi, \tau, \{\gamma_D\}, \beta) \\ = \mathcal{L}_{cls}(\phi, \gamma) + \mathcal{L}_{reg}(\phi, \beta) \\ + \alpha_1 \mathcal{L}_{dadv}(\phi, \psi) + \alpha_2 \mathcal{L}_{dins}(\phi, \tau) \\ + \alpha_3 \mathcal{L}_{cst}(\phi, \beta) + \alpha_4 \mathcal{L}_{erc}(\phi, \{\gamma_D\}) \end{aligned} \quad (22)$$

where $\alpha_1, \alpha_2, \alpha_3, \alpha_4$ represent the regularisation constants and \mathcal{L}_{reg} the bounding box regression loss. It is important to note that the features learned via the maximisation of the domain specific classification loss \mathcal{L}_{erc} can have a negative impact on the classifier $c(F; \gamma)$, and on the bounding box predictor $b(F; \beta)$, and thus can result in instability during the min-max optimisation of Eq. (22). To overcome this drawback, following [77], we introduce $|\mathbf{D}|$ additional domain-specific classifiers, $c(F; \gamma'_D)$, with a **new cross-entropy loss** \mathcal{L}_{cel} :

$$\mathcal{L}_{cel}(\phi, \{\gamma'_D\}) = - \sum_D \langle \log Q(C|B, \bar{F})|D; \gamma'_D \rangle - \sum_D \sum_{D' \neq D} \langle \log Q(C|B, F)|D'; \bar{\gamma}'_D \rangle \quad (23)$$

where the bar above \bar{F} and $\bar{\gamma}'_D$ indicates that the parameters are fixed during training.

4.3 Combined loss function

The combined loss function \mathcal{L} that we use to train the system is:

$$\begin{aligned} \mathcal{L}(\phi, \beta, \gamma, \psi, \tau, \{\gamma_D\}, \{\gamma'_D\}) = \mathcal{L}_{cls}(\phi, \gamma) + \mathcal{L}_{reg}(\phi, \beta) + \alpha_1 \mathcal{L}_{dadv}(\phi, \psi) \\ + \alpha_2 \mathcal{L}_{dins}(\phi, \tau) + \alpha_3 \mathcal{L}_{cst}(\phi, \beta) \\ + \alpha_4 \mathcal{L}_{erc}(\phi, \{\gamma_D\}) + \alpha_5 (\mathcal{L}_{cel}(\phi, \{\gamma'_D\})) \end{aligned} \quad (24)$$

where α_5 is the regularisation constant associated with the additional $|\mathbf{D}|$ domain specific classifiers γ'_D .

To minimize Eq. (24) we require,

$$\min_{\phi, \gamma, \beta, \{\gamma'_D\}} \max_{\psi, \{\gamma_D\}, \tau} \mathcal{L}(\phi, \beta, \gamma, \psi, \tau, \{\gamma_D\}, \{\gamma'_D\}) \quad (25)$$

4.4 Combined loss minimising DG trainer

Since the additional $|\mathbf{D}|$ classifiers \bar{F} and $\bar{\gamma}'_D$ are domain-specific, there is a high likelihood that they can prevent the learning of domain invariant features, which is against the goal of domain generalisation. But at the same time, the inclusion of the γ'_D classifiers can help in overcoming the instability introduced by the γ_D classifiers. Hence, an effective strategy for training these domain-specific classifiers is of crucial importance. To this end, we initially freeze ϕ and train each of the γ'_D classifiers by using data from domain D . This step will aid the domain-specific classifiers to learn only domain invariant features. In the next step, we fix all $|\mathbf{D}|$ parameters γ'_D and fine tune ϕ so that a sample I_D from domain D is classified accurately by all $\gamma'_{D' \neq D}$.

A complete DG trainer which minimises \mathcal{L} from Eq. (24) is described in Algorithm 1, which optimises the main detector to achieve domain invariant bounding box prediction performance; which is further used for achieving class-conditional invariance.

A block diagram implementing the algorithm is given in Fig. 3. Compared against any generic object detector (one or two-stage), it introduces two new modules related to class-conditional invariance and bounding box invariance, which aid to optimise the feature extractor, in order to map the input images into feature vectors so that the detection is consistent across multiple domains. The min-max optimisation is a form of adversarial learning which may be implemented by GRLs [62], which simply flip the sign of the error terms during loss backpropagation.

5 Experimental Validation

Datasets: We demonstrate the generalisation ability of our approach on the following popular multi-source object detection datasets. As it is commonly practised in the state-of-the-art, we employ the official training set (source

Algorithm 1: Training strategy for domain generalised object detection.

Input: $|D|$ domain training datasets, X_D **Input:** $\alpha_1, \alpha_2, \alpha_3, \alpha_4, \alpha_5$

Input: Feature and classifier functions f, c, b

Output: trained model ϕ, γ, β

for each epoch do

 Sample data from each training dataset respectively

 Update $\phi, \beta, \gamma, \psi, \tau$ by optimising first five terms of Eq. (24)

for each domain D do

 Sample data from the D -th dataset X_D

 Update γ'_D by optimising the \mathcal{L}_{cel} term of Eq. (24)

 Update ϕ, γ_D by optimising the \mathcal{L}_{erc} term of Eq. (24)

 Sample data from datasets $X_{D' \neq D}$

 Update ϕ by optimising the \mathcal{L}_{cel} term of Eq. (24)

end

end

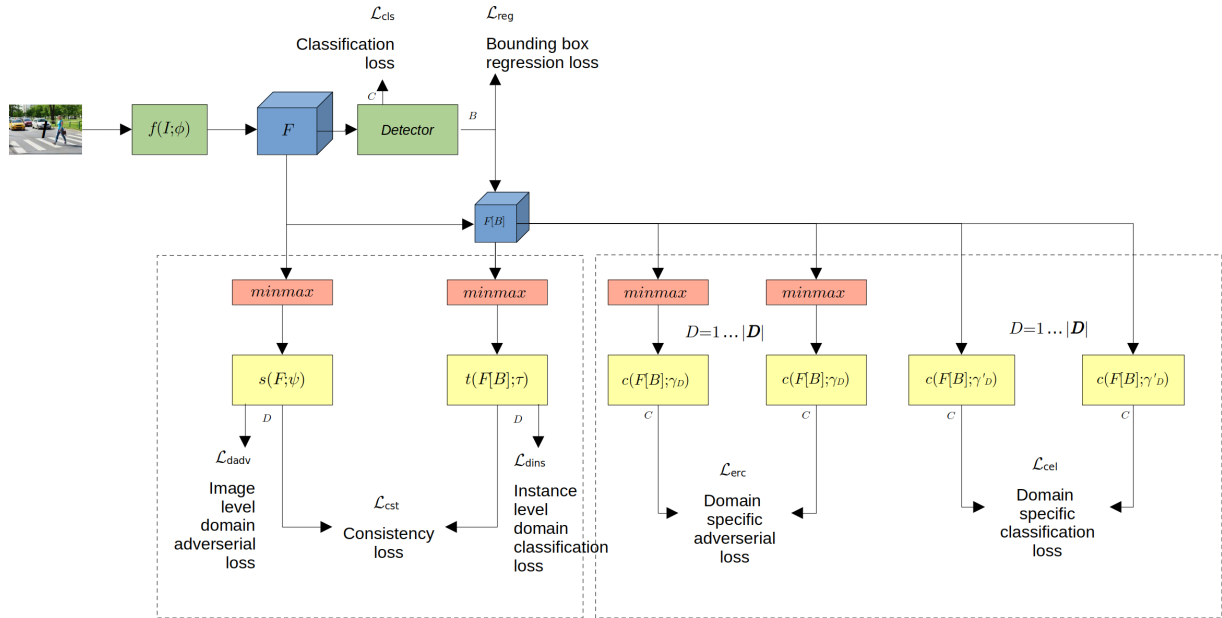


Figure 3: Block diagram of the proposed approach.

Table 1: Number of instances of each class for all autonomous driving datasets

| Dataset | person | rider | car | truck | bus | train | motorcycle | bicycle |
|------------|--------|-------|--------|-------|-------|-------|------------|---------|
| ACDC | 2221 | 276 | 8522 | 643 | 217 | 258 | 210 | 482 |
| BDD10k | 11140 | 516 | 82712 | 4266 | 1857 | 72 | 443 | 930 |
| Cityscapes | 107065 | 11815 | 159110 | 2910 | 2415 | 970 | 4440 | 24520 |
| IDD | 60617 | 73306 | 69929 | 20448 | 9540 | 15 | 83062 | 1905 |
| Total | 181043 | 85913 | 250344 | 28267 | 14031 | 1315 | 88155 | 27837 |

domain(s)) of each dataset for training and validation purposes, all the while the official validation set (target domain(s)) is reserved exclusively for testing, unless otherwise specified.

Cityscapes: Cityscapes [86] deals with the semantic understanding of urban street scenes. It has a total of 2975 images (from 18 cities) for training and 500 validation images (from 3 cities). In order to conduct a fair comparison, we resize the original images to 600×1200 pixel resolution. Cityscapes contains 8 classes: person, rider, car, truck, bus, train, motor, bike which are shared with other autonomous driving datasets. The number of instances across classes (for this and all other autonomous driving datasets used in our experiments) is shown in Table 1. *Foggy Cityscapes* has been derived from Cityscapes via synthetic fog simulation [87].

BDD10k [88]: Has been proposed along with *BDD100k* for segmentation, and overlaps with it significantly. The annotations are collected on six different scene types, six different weather conditions, and three distinct times of the day. Unlike *Foggy Cityscapes* [87], the fog in BDD10k is real. The train and validation sets have 7000 and 1000 images respectively. The segmentation masks are converted into bounding boxes to fit the object detection setting.

ACDC [89]: Adverse Conditions Dataset with Correspondences is an autonomous driving dataset targeted towards improving the performance of semantic segmentation task in adverse weather conditions. It has a total of 2006 images which are uniformly spread across fog, nighttime, rain and snow conditions. We use the standard train validation split that comes with the dataset (1600 for training and 406 for validation).

IDD [90]: Indian Driving Dataset (Parts I and II) aims for improved autonomous navigation and detection in unstructured environments. It has a total of 16063 images, split into 14027 and 2036 samples for training and validation respectively. They have been captured from 182 driving sequences on Indian roads and are annotated with 34 classes.

GWHD [91]: The goal of the Global Wheat Head Detection dataset is to accurately detect the wheat heads from optical images captured via a wide variety of platforms, and camera settings, with additional variation in wheat genotype, sowing density, growth stage and soil type. It consists in a total of 6000 images (resolution: 1024×1024 pixels) acquired across 47 different sessions; with each being restricted to a single domain/farm. The training set has 18 domains with a total of 2943 images while the validation set contains samples captured across 8 different sessions with 1424 images and the test set has data from 21 different sessions with a total of 1434 images. The experiments have been conducted using the aforementioned train/val/test split.

URPC 2019 [14]: This underwater dataset contains 3765 images for training and 942 for validation with its highest resolution being 3840×2160 pixels, as captured by a GoPro camera. Five classes are present: echinus (18490), starfish (5794), holothurian (5199), scallop (6617) and waterweeds (82), where the numbers in parenthesis denote the respective number of instances for each class. URPC2019 has been formed via the synthetic generation of 8 types of water quality as distinct domains using style transfer.

Setups: The following experiments have been performed in order to analyse the generalisation ability of the proposed approach across multiple object detection architectures, multiple generalisation settings, and in order to also assess their performance against existing detectors from the state-of-the-art equipped with generalisation capabilities.

1. *Multi-class, single target domain*: In this experiment, we evaluate the cross dataset generalisation ability of the object detectors used in this work. We use a leave-one-domain-out strategy across four autonomous driving datasets (*ACDC*, *BDD10K*, *Cityscapes*, *IDD*). The shift in this experiment is manifested in the form of new datasets which are captured by using completely different experiment protocols or geographical locations than the source domains. The results are presented in Table 2, where *Single-best* indicates the best performing baseline model (FCOS, YOLOv3, Faster R-CNN) after training (and validating) independently with each of the source domains and testing with the validation set of the target domain. *Source-combined* indicates the combined use of all source domains in terms of training and validation sets and once again testing with the validation set of the target domain. *Ours* denotes the same setup as *Source-combined*, with the addition of the

domain generalisation capacity to the tested detector. *Oracle-Train on Target* refers to training (and validating) using the target domain’s training set, and to testing with the target domain validation set.

2. *Single-class, multiple target domains*: The *GWHD* dataset enables evaluating the generalisation capacity of a model on a scenario with multiple target domains, where the shift in both the training and target domains stems from multiple factors such as acquisition location and equipment, soil type, wheat genotype, growth stage and sowing density (Table 3). We include qualitative examples of successful (Fig. 6) and failed (Fig. 7) detection cases, highlighting the strengths and weaknesses of the proposed approach. To the best of our knowledge, this is the only public dataset aimed at evaluating domain generalisation performance within a single dataset.
3. *Ablation studies*: This experiment aims to measure the individual as well as combined effects on performance of the proposed bounding box and class conditional alignment modules. To this end, models relying on partial losses have been trained and evaluated on both single-class/multi-target domain and multi-class/single-target domain datasets across all three tested detectors (Table 4). In addition to the aforementioned ablation experiments, we also provide a localisation performance comparison (Fig. 8).
4. *Comparison with existing approaches*: Two experiments have been conducted to this end. The first compares the proposed DGYOLO against the reported IRM based DGYOLO [14] from the state-of-the-art, using the URPC2019 dataset (Table 5). The second compares the proposed DGFR-CNN against the reported disentanglement based counterpart [18] from the state-of-the-art, using the BDD10k, Cityscapes and Foggy Cityscapes datasets (Table 6). Moreover, we highlight the limitation of the setup employed by Lin et al. [18], where 3 datasets are used, and one of them (*Foggy Cityscapes*) is directly derived from the other (*Cityscapes*). Instead, we propose using Setup-1 (presented in Table 2) as a new, more extensive benchmark for the domain generalisation setting, as it employs 4 distinct datasets.

Network Architectures: We instantiate the general structure of Fig. 3 using three different, neural network-based detectors, each extended with the new losses as additional neural network loss heads, and with GRLs to implement the adversarial learning (minmax).

The three baseline models (Faster R-CNN, YOLOv3, FCOS) share some structures but have various small differences, to optimise their individual performances. These optimisations are then retained into the DG versions. The number and sizes of layers used in our instance classifiers differs slightly across the models, to match the size of the feature maps from the baseline models. Training algorithms and parameters are also taken from the original model papers.

FRCNN [4] is a two-stage detector, instantiated in the DG framework as in fig. 4. We here use a ResNet50-FPN backbone network initialised with pre-trained pretrained COCO weights [8] for the autonomous driving experiments, and ImageNet weights [35] for GWHD. The feature extractor f is the backbone, region proposal network and ROI pooling layer of the Faster R-CNN network. b is the bounding box regressor and c is the instance-level classifier components of the Faster R-CNN. The output F of the backbone network is fed as input to domain adversarial network $s(F; \psi)$ while the output of ROI Pooling layer of the Faster R-CNN detector is fed as an input to instance level domain classifier $t(F[B]; \tau)$, $2|D|$ domain specific classifiers (γ_D and γ'_D). All terms in the loss function described in Eq. (24) correspond to either a domain or object classifier. We use cross-entropy to train each of these classifier modules. The resulting network is shown in Fig. 4. *Training*: from empirical observations, the optimal values of the regularisation constants were found to be $\alpha_1 = 1$, $\alpha_2 = 0.1$, $\alpha_3 = 1$, $\alpha_4 = 0.001$, and $\alpha_5 = 0.05$. More details about the choice of regularisation constants can be found in supplementary material. We used early stopping with a patience of 10 epochs. AdamW (weight decay = 0.0005, learning rate = 0.001, batchsize=2) has been used as optimiser while training with GWHD and Stochastic Gradient Descent (SGD) (weight decay = 0.0005, momentum=0.9, learning rate= 2×10^{-3} , batchsize=2) has been used for other datasets (Cityscapes, BDD100K).

YOLOv3 [25, 26] is a single-stage detector, which means that B and C are assumed to be independent given F and D , i.e. $P(B, C|F, D) = P(B|F, D)P(C|F, D)$, resulting in the network structure of Fig. 5 We here use a DarkNet-53 backbone network initialise with pretrained weights. The feature extractor F is the top level of the backbone, evaluated at a set of anchor points. Training used a SGD optimiser (learning rate = 0.1, weight decay = 0.0005, momentum = 0.9, batchsize=8) for autonomous driving datasets, while Adam optimiser (learning rate = 0.001, weight decay = 0.0005) was used for GWHD and URPC datasets.

FCOS [27] is another single-stage detector, so shares the same network structure as Fig. 5. The backbone used is ResNet50. F is defined as the contents of the top *three* layers of the backbone network, plus five further layers linked from them and to each other, with the bounding box and classification heads swept over each of these. (An additional centerness head is also used to weight which detections to report). Training is using gradient descent. From empirical observations, we set the regularisation constants to $\alpha_1 = 1$, $\alpha_2 = 0.1$, $\alpha_3 = 1$, $\alpha_4 = 0.001$, and $\alpha_5 = 0.05$. We used early stopping with a patience of 10 epochs. AdamW (weight decay = 0.0001, learning rate = 0.0001, batchsize=8) has been used as optimiser while training with GWHD and Stochastic Gradient Descent (SGD) (weight decay = 0.0001,

Domain Generalisation for Object Detection

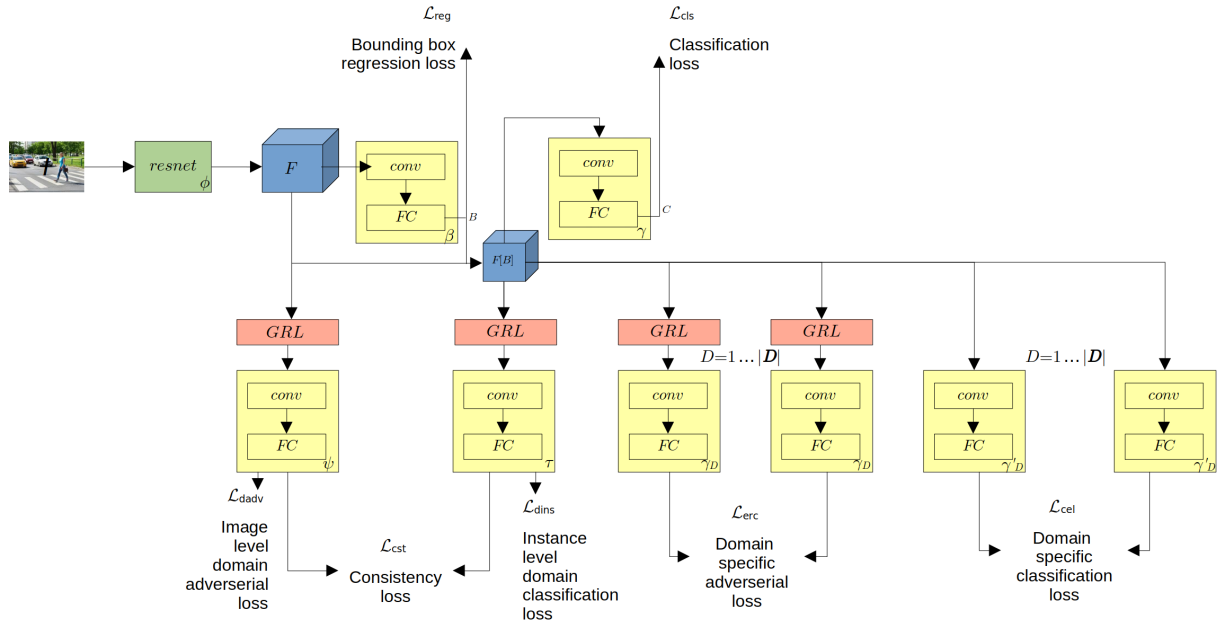


Figure 4: Block diagram of the proposed approach, instantiated as FRCNN with neural network heads.

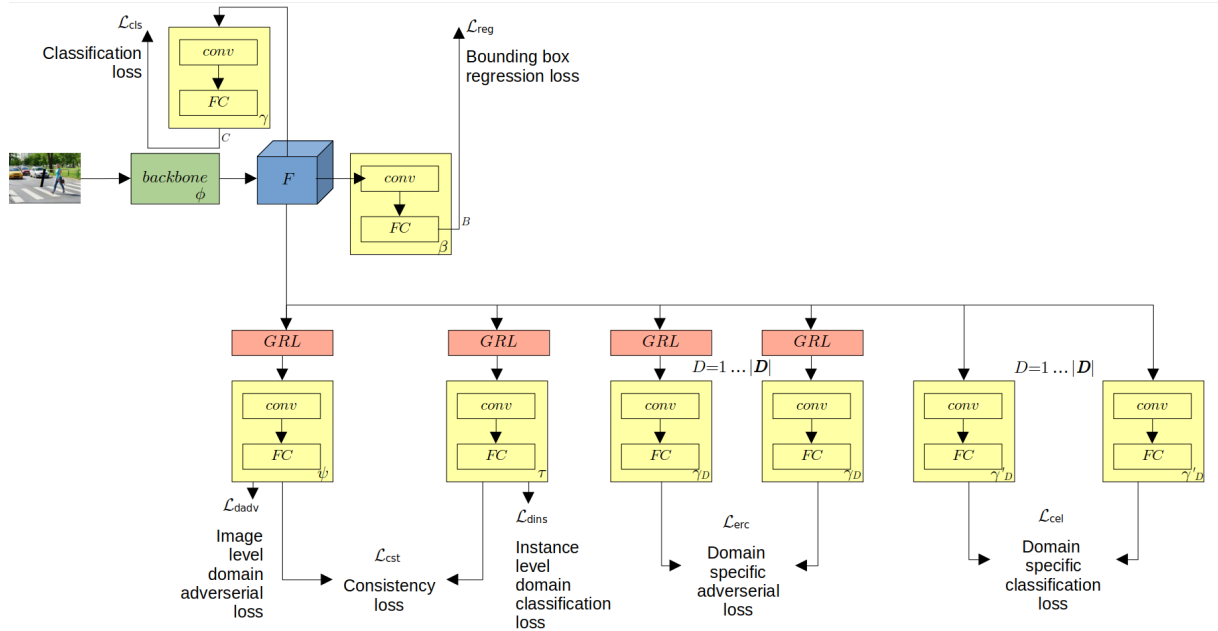


Figure 5: Block diagram of the proposed approach, instantiated as single stage detector with neural networks. For YOLOv3, the backbone is DarkNet-53 and F is the top layer of this backbone around an anchor; For FCOS the backbone is ResNet50 and F is a feature pyramid around a pixel location.

momentum=0.9, learning rate=0.01, batchsize=8) has been used for autonomous driving datasets. The feature extractor F is the top level of the backbone, evaluated at a set of anchor points.

Hardware: The experiments were conducted on a NVIDIA RTX 3090 GPU with 24GB of memory and 10496 cores. Each epoch, including validation, lasted approximately 20 minutes.

Software: The experiments were implemented using the PyTorch deep learning framework and FRCNN, YOLO and FCOS models from the Torchvision library, modified with DG extensions. The modified code is GPLv3 open source and made available with instructions to replicate all experiments at <https://github.com/karthikiitm87/DG0D>.

Metrics: We follow the standard practice for measuring performance of object detection tasks, and report *mean Average Precision* (mAP) at 50% *Intersection over Union* (IoU) – mAP@50 [7] (mAP for short) as our main performance metric.

Every output from the detector is assigned a confidence score $p \in [0, 1]$, and, for every class $C \in \mathbf{C}$, *precision* and *recall* values are calculated at every confidence level T , by dividing the detector outputs into *true positives* ($TP_{C,T}$) and *false positives* ($FP_{C,T}$) according to IoU with the ground truth. Detector outputs with $p \geq T$ and overlap with the ground truth of the same class higher or equal to $\text{IoU} = 50\%$ are deemed ($TP_{C,T}$), and all others ($FP_{C,T}$). Any ground truth annotation which was not matched with a detector output is deemed a *false negative* ($FN_{C,T}$). Finally, for each class C and at each confidence level T , *precision* is defined as a fraction of correct detector outputs:

$$p_{C,T} = \frac{TP_{C,T}}{TP_{C,T} + FP_{C,T}}, \quad (26)$$

and *recall* as a fraction of ground truth objects which were correctly detected:

$$r_{C,T} = \frac{TP_{C,T}}{TP_{C,T} + FN_{C,T}}. \quad (27)$$

This allows us to further define *precision at r* , as the precision value corresponding to a certain recall level r :

$$p_C(r) = p_{C,T} \text{ s.t. } r_{C,T} = r, \quad (28)$$

as well as *interpolated precision*, corresponding to the maximum value of precision at every recall level, and required to remove the sensitivity of precision and recall measures to ranking differences (i.e. the sample order during evaluation):

$$\tilde{p}_C(r) = \max_{r' \geq r} p_C(r'). \quad (29)$$

The pairs of (interpolated) precision and recall values at different confidence scores are used to calculate the precision-recall curve for each class. *Average Precision* for class C (AP_C) summarises the shape of the precision-recall curve for each class across all confidence levels (in our case, calculated as an 101-point approximation), corresponding to the area under the curve (calculated at $\text{IoU} = 50\%$):

$$AP_C = \frac{1}{101} \sum_{\substack{i=0 \\ r=0.01i}}^{100} \tilde{p}_C(r). \quad (30)$$

Finally, mAP is calculated as the mean of AP_C for all classes C present in the dataset:

$$\text{mAP} = \frac{1}{|\mathbf{C}|} \sum_{C \in \mathbf{C}} AP_C. \quad (31)$$

6 Results

Multi-class, single target domain. These experiments, using multiple autonomous driving datasets, are presented in Table 2. It can be seen that the addition of our proposed alignment modules during the training phase results in a consistent performance improvement over both the *Single-best* and *Source-combined* (except for the FCOS detector in the case of $(C, I, A) \rightarrow B$; however in this case the difference between *Source-combined*, *Oracle* and our proposed approach is less than a single percentage point). In fact, we also surpass the *Oracle* in 5 distinct experiments, most notably in 3 out of 4 experiments with YOLOv3 architecture. While the per-class improvement is not achieved in all cases, our proposal improves the performance on half or more classes present in the datasets in 10 out of 12 cases. It is worth noting that the results for the *train* class are overall quite poor, across all settings, as this class was severely underrepresented across all datasets.

Table 2: Cross dataset generalisation performance on ACDC (A), BDD10K (B), Cityscapes (C), IDD (I). The best AP and mAP in each setting (excluding *Oracle*) is highlighted in bold. $(X, Y, Z) \rightarrow W$: X, Y, Z refer to the source domains, and W denotes the target domain. See the text for details on the train/validation/test split strategies.

| DG Setting | Methods | person | rider | car | truck | bus | train | motor | bike | mAP |
|---------------------------|------------------------|--------------|--------------|--------------|--------------|--------------|--------------|--------------|--------------|--------------|
| FCOS | | | | | | | | | | |
| (A, B, C) \rightarrow I | Single-best | 24.48 | 22.02 | 48.98 | 28.13 | 16.53 | 0.00 | 21.01 | 1.99 | 20.39 |
| | Source-combined | 29.32 | 29.01 | 50.75 | 29.40 | 14.38 | 0.00 | 31.35 | 13.01 | 24.65 |
| | DGFCOS (Ours) | 28.73 | 28.65 | 47.96 | 29.63 | 18.59 | 0.00 | 30.93 | 14.74 | 24.90 |
| | Oracle-Train on Target | 44.45 | 50.35 | 62.81 | 57.95 | 53.88 | 0.00 | 52.79 | 28.77 | 43.87 |
| (B, C, I) \rightarrow A | Single-best | 35.56 | 16.82 | 65.29 | 21.15 | 05.43 | 0.00 | 23.94 | 08.19 | 22.05 |
| | Source-combined | 41.71 | 21.14 | 73.96 | 34.30 | 13.30 | 17.53 | 28.95 | 12.23 | 30.39 |
| | DGFCOS (Ours) | 44.08 | 18.24 | 73.37 | 36.17 | 13.13 | 19.73 | 29.35 | 13.39 | 30.93 |
| | Oracle-Train on Target | 36.08 | 10.55 | 65.48 | 19.17 | 10.63 | 24.03 | 12.91 | 04.49 | 22.92 |
| (C, I, A) \rightarrow B | Single-best | 51.60 | 29.06 | 59.79 | 14.84 | 19.25 | 0.00 | 24.89 | 25.41 | 28.10 |
| | Source-combined | 54.48 | 37.98 | 62.70 | 18.64 | 21.99 | 7.43 | 33.48 | 25.27 | 32.75 |
| | DGFCOS (Ours) | 54.81 | 40.00 | 62.91 | 16.83 | 24.17 | 0.33 | 30.50 | 27.23 | 32.10 |
| | Oracle-Train on Target | 51.36 | 29.91 | 67.19 | 30.83 | 31.32 | 0.65 | 22.66 | 23.69 | 32.20 |
| (I, A, B) \rightarrow C | Single-best | 43.41 | 41.23 | 63.19 | 25.26 | 43.99 | 0.00 | 35.46 | 30.20 | 35.34 |
| | Source-combined | 47.57 | 48.60 | 69.02 | 36.19 | 48.59 | 13.68 | 34.11 | 34.54 | 41.54 |
| | DGFCOS (Ours) | 46.91 | 45.51 | 72.50 | 37.32 | 52.21 | 11.93 | 32.55 | 37.26 | 42.02 |
| | Oracle-Train on Target | 50.08 | 51.66 | 68.46 | 23.63 | 51.72 | 14.18 | 35.60 | 43.70 | 42.38 |
| YOLOv3 | | | | | | | | | | |
| (A, B, C) \rightarrow I | Single-best | 9.10 | 1.80 | 40.73 | 10.12 | 6.74 | 0.00 | 2.77 | 2.13 | 9.17 |
| | Source-combined | 15.87 | 9.34 | 40.11 | 13.35 | 9.92 | 0.00 | 13.49 | 9.28 | 13.92 |
| | DGYOLO (Ours) | 15.97 | 9.09 | 40.34 | 14.32 | 10.92 | 0.00 | 13.63 | 11.14 | 14.43 |
| | Oracle-Train on Target | 26.39 | 37.92 | 53.05 | 42.07 | 43.51 | 0.00 | 48.91 | 16.49 | 33.54 |
| (B, C, I) \rightarrow A | Single-best | 13.55 | 10.50 | 50.14 | 10.67 | 07.53 | 0.00 | 30.88 | 4.75 | 16.00 |
| | Source-combined | 23.04 | 17.22 | 62.32 | 21.03 | 16.49 | 0.00 | 18.54 | 10.99 | 21.20 |
| | DGYOLO (Ours) | 20.47 | 20.64 | 65.81 | 30.45 | 18.75 | 0.00 | 11.31 | 10.91 | 22.29 |
| | Oracle-Train on Target | 12.26 | 2.97 | 54.12 | 8.02 | 5.94 | 7.78 | 9.62 | 6.85 | 13.44 |
| (C, I, A) \rightarrow B | Single-best | 29.90 | 11.54 | 47.31 | 7.39 | 12.05 | 0.00 | 28.71 | 7.08 | 18.00 |
| | Source-combined | 40.19 | 25.41 | 54.10 | 08.04 | 11.44 | 0.00 | 28.52 | 14.10 | 22.72 |
| | DGYOLO (Ours) | 40.00 | 31.37 | 53.68 | 8.85 | 9.88 | 0.00 | 33.36 | 15.45 | 24.07 |
| | Oracle-Train on Target | 23.21 | 08.91 | 53.07 | 16.65 | 17.23 | 0.00 | 10.89 | 08.25 | 17.28 |
| (I, A, B) \rightarrow C | Single-best | 18.24 | 11.48 | 44.58 | 15.21 | 34.49 | 0.00 | 26.20 | 07.44 | 19.70 |
| | Source-combined | 24.90 | 24.16 | 54.14 | 28.81 | 43.97 | 0.00 | 30.24 | 17.98 | 28.02 |
| | DGYOLO (Ours) | 22.82 | 24.69 | 56.29 | 32.32 | 43.16 | 0.00 | 32.15 | 13.95 | 28.17 |
| | Oracle-Train on Target | 27.82 | 29.93 | 56.23 | 15.43 | 32.31 | 0.00 | 19.05 | 26.17 | 25.87 |
| Faster R-CNN | | | | | | | | | | |
| (A, B, C) \rightarrow I | Single-best | 31.61 | 26.95 | 57.34 | 32.96 | 29.67 | 0.00 | 30.42 | 16.77 | 28.21 |
| | Source-combined | 35.17 | 30.68 | 56.84 | 34.21 | 28.80 | 0.00 | 35.74 | 18.79 | 30.03 |
| | DGFR-CNN (Ours) | 33.64 | 29.65 | 57.66 | 36.53 | 29.84 | 0.00 | 34.42 | 21.27 | 30.38 |
| | Oracle-Train on Target | 44.20 | 50.81 | 64.44 | 56.04 | 52.32 | 0.00 | 58.23 | 28.92 | 44.37 |
| (B, C, I) \rightarrow A | Single-best | 33.59 | 18.86 | 71.61 | 26.06 | 14.08 | 35.63 | 27.93 | 10.71 | 29.81 |
| | Source-combined | 41.09 | 18.51 | 72.36 | 43.39 | 24.77 | 26.50 | 38.81 | 12.54 | 34.75 |
| | DGFR-CNN (Ours) | 42.03 | 20.61 | 74.57 | 43.18 | 25.90 | 29.58 | 40.68 | 11.42 | 36.00 |
| | Oracle-Train on Target | 40.83 | 28.75 | 73.32 | 37.77 | 32.51 | 49.39 | 38.56 | 15.57 | 39.59 |
| (C, I, A) \rightarrow B | Single-best | 53.39 | 26.40 | 61.71 | 19.43 | 26.62 | 0.00 | 35.50 | 17.90 | 30.14 |
| | Source-combined | 58.59 | 45.75 | 65.39 | 25.74 | 27.74 | 8.70 | 37.38 | 16.32 | 34.72 |
| | DGFR-CNN (Ours) | 58.67 | 47.00 | 65.53 | 24.44 | 25.90 | 9.91 | 40.83 | 19.10 | 35.31 |
| | Oracle-Train on Target | 55.19 | 33.55 | 69.43 | 38.04 | 37.74 | 0.00 | 32.54 | 21.71 | 36.02 |
| (I, A, B) \rightarrow C | Single-best | 39.76 | 30.74 | 61.55 | 35.32 | 40.29 | 37.70 | 26.95 | 32.17 | 38.06 |
| | Source-combined | 48.80 | 43.07 | 69.68 | 42.73 | 55.33 | 2.48 | 44.23 | 34.22 | 42.57 |
| | DGFR-CNN (Ours) | 49.46 | 42.76 | 70.26 | 42.54 | 56.01 | 12.62 | 44.16 | 37.11 | 44.36 |
| | Oracle-Train on Target | 54.51 | 51.10 | 73.84 | 42.01 | 58.75 | 47.72 | 44.06 | 47.33 | 52.42 |

Single-class, multiple target domains. This experiment allows us to examine the effect of our proposed method in the case where a trained model is deployed on multiple target domains at once. The results, detailed in Table 3, show that the addition of our modules on top of all three baseline architectures (Faster R-CNN, FCOS, YOLOv3 trained on all available training data, equivalent to the *Source-combined* setting in the multi-class experiment) increases overall

performance. Further, it can also be seen that while the improvement is not as consistent across the domains in case of Faster R-CNN where the performance improves on just over half (11/21) of the domains, the improvement is much more consistent for both FCOS (17/21 domains) and YOLOv3 (19/21 domains) architectures. This may indicate that our method is more beneficial to the performance of single-stage detector architectures than that of two-stage architectures, possibly because the instance-level alignment still acts on the features of the whole image (unlike with two-stage approaches, where instance-level alignment acts only on the features contained within the object bounding box). We also show example detector outputs both for successful detections (Fig. 6) and failure cases (Fig. 7). Fig. 6 indicates at the improved localisation performance across all baseline approaches (discussed in the next paragraph). The examples in Fig. 7 show that all approaches produce false detections when the background (twigs, textures and shadows in Fig. 7 (a), (b) and (d)) resembles the target class (wheat head), and struggle in dense regions with many objects and mutual occlusions (Fig. 7 (c)).

Table 3: Performance improvement per domain in terms of mAP, of the proposed framework over baselines from different networks (Faster R-CNN, FCOS, YOLOv3) on GWHD.

| Domain ID | # of Images | Faster R-CNN | DGFR-CNN | FCOS | DGFCOS | YOLOv3 | DGYOLO |
|-------------|-------------|--------------|----------------------|--------------|----------------------|--------------|---------------------|
| 26 | 22 | 39.27 | 40.87 (+1.60) | 44.49 | 47.93 (+3.44) | 38.42 | 44.03 (+5.61) |
| 27 | 16 | 92.57 | 92.81 (+0.24) | 93.14 | 80.46 (-12.68) | 92.67 | 93.85 (+1.08) |
| 28 | 14 | 50.59 | 54.82 (+4.23) | 52.67 | 55.69 (+3.02) | 54.97 | 66.37 (+11.40) |
| 29 | 30 | 66.46 | 63.77 (-2.69) | 63.37 | 66.91 (+3.54) | 65.04 | 67.30 (+2.26) |
| 30 | 30 | 48.22 | 48.63 (+0.41) | 43.49 | 47.48 (+3.99) | 42.82 | 52.71 (+9.89) |
| 31 | 30 | 72.29 | 64.86 (-7.43) | 73.60 | 74.16 (+0.56) | 72.51 | 73.25 (+0.74) |
| 32 | 17 | 67.74 | 70.25 (+2.51) | 63.68 | 65.19 (+1.51) | 67.34 | 68.90 (+1.56) |
| 33 | 41 | 50.84 | 50.61 (-0.23) | 49.48 | 51.06 (+1.58) | 50.51 | 52.15 (+1.64) |
| 34 | 33 | 49.79 | 49.59 (-0.20) | 48.06 | 49.40 (+1.34) | 49.60 | 51.10 (+1.50) |
| 35 | 106 | 52.26 | 52.24 (-0.02) | 48.98 | 51.02 (+2.04) | 52.34 | 54.69 (+2.35) |
| 36 | 84 | 39.91 | 39.65 (-0.26) | 36.60 | 37.37 (+0.97) | 40.13 | 41.74 (+1.61) |
| 37 | 144 | 22.11 | 21.97 (-0.14) | 23.14 | 23.81 (+0.67) | 24.37 | 24.97 (+0.60) |
| 38 | 106 | 17.17 | 16.99 (-0.18) | 13.00 | 12.26 (-0.74) | 20.05 | 20.85 (+0.80) |
| 39 | 100 | 51.94 | 55.54 (+3.60) | 49.74 | 57.94 (+8.20) | 49.94 | 55.59 (+5.65) |
| 40 | 100 | 55.26 | 57.37 (+2.11) | 57.72 | 62.99 (+5.27) | 55.05 | 61.10 (+6.05) |
| 41 | 95 | 50.42 | 55.65 (+5.23) | 48.88 | 55.38 (+6.50) | 48.27 | 55.54 (+7.27) |
| 42 | 60 | 43.96 | 50.34 (+6.37) | 41.14 | 49.25 (+8.11) | 40.74 | 48.99 (+8.25) |
| 43 | 69 | 50.20 | 52.90 (+2.70) | 49.77 | 52.09 (+2.32) | 48.90 | 51.95 (+3.05) |
| 44 | 77 | 67.56 | 66.60 (-0.94) | 68.01 | 68.18 (+0.17) | 68.03 | 69.59 (+1.56) |
| 45 | 60 | 55.68 | 57.04 (+1.36) | 55.58 | 54.47 (-1.11) | 62.25 | 58.91 (-3.34) |
| 46 | 200 | 77.59 | 76.49 (-1.10) | 77.17 | 74.18 (-2.99) | 77.78 | 77.02 (-0.76) |
| Mean | | 53.42 | 54.24 (+0.82) | 52.46 | 54.15 (+1.69) | 53.42 | 56.7 (+3.28) |

Ablation studies. To study the effect of different loss components on the overall model performance, we repeat the experiments from Tables 2 (selecting two out of four target domains) and 3, while relying on a partial loss function to optimise the network weights. These results, reported in Table 4, show that the best performance was achieved when all the proposed loss functions were combined together. Further, it can also be seen that while performing the alignment across all domains simultaneously at both the image and the instance level (second row) improves performance, as does domain-specific alignment (third row), the combination of all the proposed losses, which fully addresses both the covariate and concept shift, is needed to achieve the best performance.

To further study the effect of our proposed method on the three baseline architectures, we consider the performance of our models on the GWHD dataset at different IoU levels. The single-class dataset was selected for this experiment, as in this case, AP_C is equivalent to the overall mAP. We show the *precision-recall (PR) curves* (which are the basis of calculating AP_C) across three different IoU levels (10%, 50% and 75%) for all models in Fig. 8. The area under the curve on all PR curves at all IoU levels is higher when adding our proposed modules (full lines) to all baseline models (dotted lines), indicating that our approach consistently improves detector localisation.

Comparison with existing approaches. A comparison of DGYOLO with the approach proposed by Liu et al. [14] is shown in Table 5. It can be seen that our proposed DGYOLO improves performance over the existing approach [3] by 1.35 mAP, improving the performance on 5 out of 6 classes in the dataset. Table 6 shows the comparison of DGFR-CNN with the disentanglement-based approach [18], where we report an improvement in mAP on 2 out of 3 datasets (BDD10k: +2.2, FoggyCityscapes: +1.6, Cityscapes: -1.3). Individual class performance indicates that our proposed DGFR-CNN struggles on the minority class (*train*), impacting the overall mAP on Cityscapes and

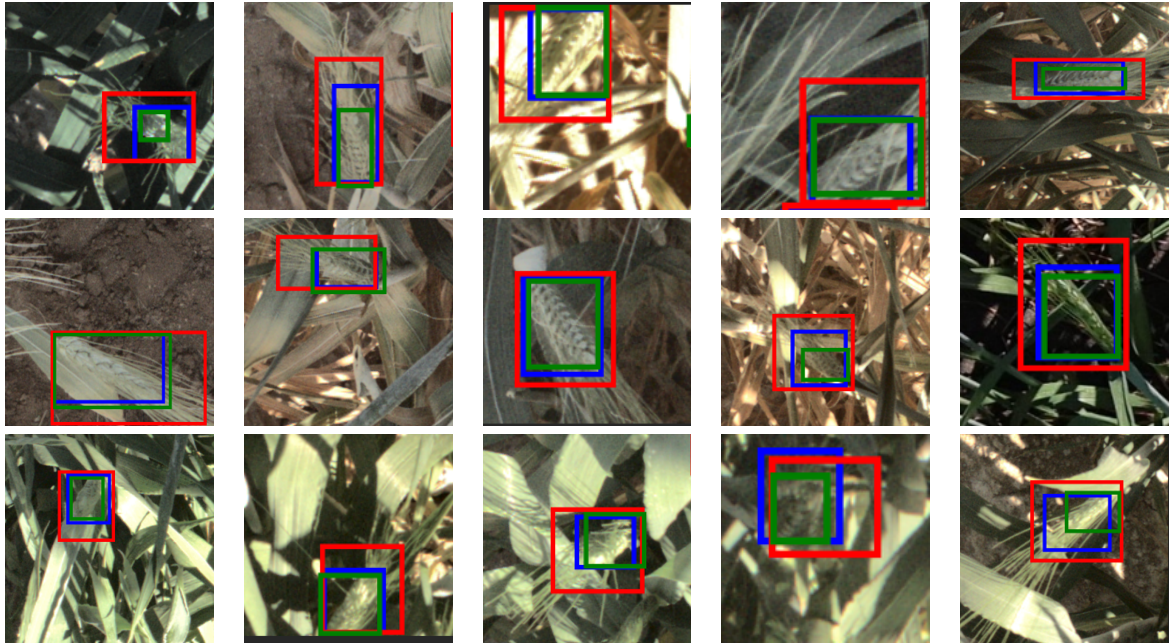


Figure 6: Localisation performance of proposed DG framework on GWHD 2021 dataset. Output of: First row: FCOS vs DGFCOS. Second row: YOLOv3 vs DGYOLO. Third row: Faster R-CNN vs DGFR-CNN. Color codes: Ground truth ■, Baseline ■ and DG framework ■.

Table 4: Ablation study of the proposed approach on the GHWD dataset, and two out of four autonomous driving experiments (*IDD* (I), *Cityscapes* (C) and *BDD10K* (B)). The left and right sides of \rightarrow indicate the source and target datasets, respectively). BBA: Bounding Box Alignment. CCA: Class Conditional Alignment. The best results are highlighted in bold. Results are reported in terms mAP values.

| Baseline | BBA | CCA | GWHD | | | (A, B, C) \rightarrow I | | | (B, C, I) \rightarrow A | | |
|------------------------|--|------------------------|--------------|--------------|--------------|---------------------------|--------------|--------------|---------------------------|--------------|--------------|
| L_{cls} L_{reg} | L_{dadv} L_{dinst} L_{cst} | L_{erc} L_{cel} | FCOS | YOLOv3 | Faster R-CNN | FCOS | YOLOv3 | Faster R-CNN | FCOS | YOLOv3 | Faster R-CNN |
| + | - | - | 59.24 | 44.44 | 56.24 | 24.65 | 13.92 | 30.03 | 30.39 | 21.20 | 34.75 |
| + | + | - | 59.45 | 45.62 | 56.80 | 24.73 | 13.99 | 30.10 | 30.42 | 21.52 | 35.12 |
| + | - | + | 59.85 | 45.12 | 56.54 | 24.70 | 14.02 | 30.19 | 30.51 | 21.75 | 35.25 |
| + | + | + | 60.67 | 46.54 | 57.42 | 24.90 | 14.43 | 30.38 | 30.93 | 22.29 | 36.00 |

FoggyCityscapes. We do not perform these experiments using any other baseline models, as the existing approaches [14, 18] only apply to a single baseline architecture (YOLOv3 and Faster R-CNN respectively).

7 Conclusion

We propose a domain generalisation approach for object detection, which addresses both constituent components of domain shift (i.e. covariate and concept shift), based on a rigorous mathematical analysis. This is implemented as feature alignment achieved through GRL [62]. We demonstrate how our proposed method can be applied to both single-stage (YOLOv3, FCOS) and two-stage (Faster R-CNN) object detection architectures, as the first architecture-agnostic DG-OD approach. We provide a comprehensive evaluation on both autonomous driving and precision agriculture datasets, showing improved domain generalisation and localisation performance compared to baseline architectures. We study the effect of our proposed modules in an ablation study to conclude that all proposed modules are required to address domain shift in full. Finally, we also outperform the state-of-the-art approaches [14, 18] on their own benchmarks, and propose a new and extended benchmark setup for evaluating domain generalisation approaches for object detection in autonomous driving, relying on 4 distinct dataset. Possible future directions include replacing the

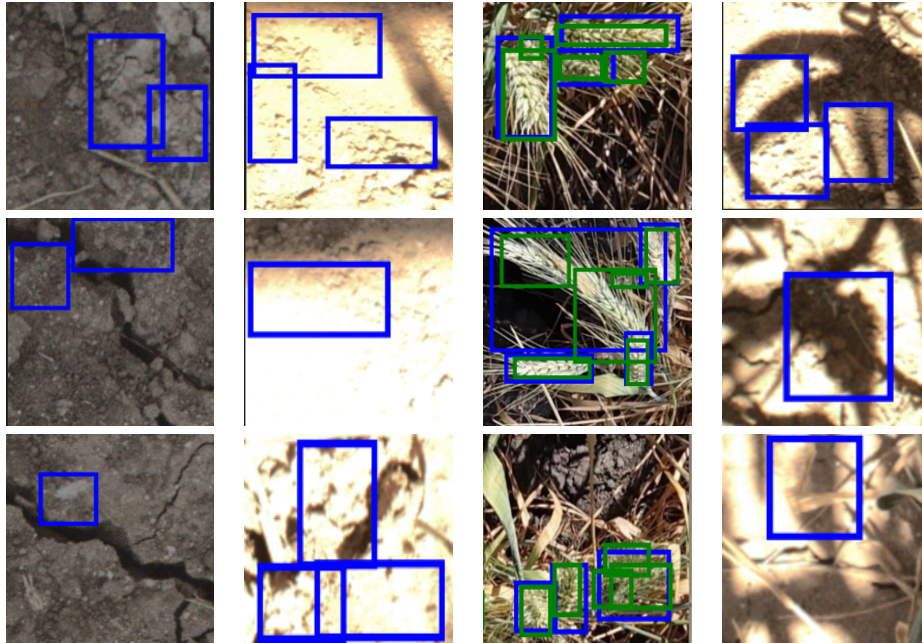


Figure 7: Failure case analysis for GWHD 2021 dataset on: First row: DGFCOS. Second row: DGYOLO. Third row: DGFR-CNN. Colour codes: Predictions ■, Ground Truth ■.

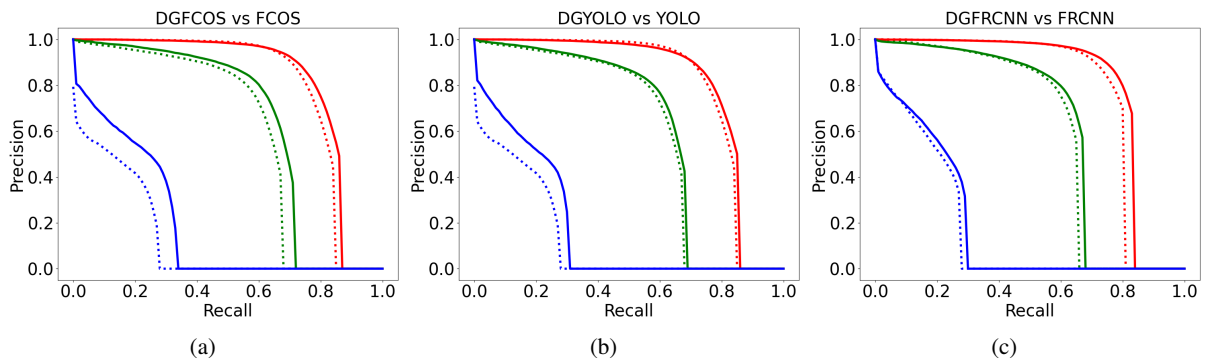


Figure 8: Precision-recall curves demonstrate an improved localisation using proposed framework for GWHD dataset. (a) DGFCOS vs FCOS, (b) DGYOLO vs YOLOv3, and (c) DGFR-CNN vs Faster R-CNN. Color codes: IoU = 0.1 ■, IoU = 0.5 ■ and IoU = 0.75 ■.

GRL [62] with different feature alignment techniques (e.g. [63, 64, 65, 66, 67]) and explicit constraints to eliminate domain specific bias.

References

- [1] Glenn Jocher, Alex Stoken, Jirka Borovec, NanoCode012, ChristopherSTAN, Liu Changyu, Laughing, tkianai, Adam Hogan, lorenzomamma, yxNONG, AlexWang1900, Laurentiu Diaconu, Marc, wanghaoyang0106, ml5ah, Doug, Francisco Ingham, Frederik, Guilhen, Hatovix, Jake Poznanski, Jiacong Fang, Lijun Yu, changyu98, Mingyu Wang, Naman Gupta, Osama Akhtar, PetrDvoracek, and Prashant Rai. ultralytics/yolov5: v3.1 - Bug Fixes and Performance Improvements, October 2020.
- [2] Mingxing Tan, Ruoming Pang, and Quoc V Le. Efficientdet: Scalable and efficient object detection. In *Proceedings of the IEEE/CVF Conference on Computer Vision and Pattern Recognition*, pages 10781–10790, 2020.

Table 5: Quantitative analysis for the proposed approach in a DG setting using the UPRC2019 underwater dataset. The best results are highlighted in bold. The scores represent the average performances for each class across 8 synthetically generated water quality domains.

| Method | echinus | starfish | holothurian | scallop | waterweeds | mAP |
|--------------------------|--------------|--------------|--------------|--------------|--------------|--------------|
| baseline(YOLOv3) | 53.51 | 7.32 | 11.15 | 9.89 | 0.00 | 16.37 |
| WQT-only | 60.98 | 17.08 | 33.29 | 39.02 | 2.38 | 30.55 |
| Faster R-CNN + FPN 29.49 | 5.91 | 9.13 | 1.07 | 10.40 | 11.23 | |
| SSD512 | 26.62 | 14.44 | 18.07 | 1.41 | 14.5 | 15.22 |
| SSD300 | 27.31 | 14.57 | 13.62 | 3.01 | 2.98 | 12.31 |
| [14] | 63.84 | 27.37 | 35.64 | 36.88 | 5.11 | 33.77 |
| DGYOLO (Ours) | 65.21 | 28.10 | 25.10 | 42.10 | 15.10 | 35.12 |

Table 6: Quantitative comparison results of the proposed approach against the one proposed by Lin *et al.* [18].

| DG Setting | Methods | person | rider | car | truck | bus | train | motor | bike | mAP |
|------------|-----------------|-------------|-------------|-------------|-------------|-------------|-------------|-------------|-------------|-------------|
| F & B to C | [18] | 43.6 | 46.2 | 63.2 | 41.9 | 60.9 | 51.1 | 36.0 | 41.3 | 47.9 |
| | DGFR-CNN (Ours) | 51.7 | 47.2 | 71.7 | 38.7 | 54.2 | 29.0 | 37.4 | 42.9 | 46.6 |
| C & B to F | [18] | 31.8 | 38.4 | 49.3 | 27.7 | 35.7 | 26.5 | 24.8 | 33.1 | 33.4 |
| | DGFR-CNN (Ours) | 38.1 | 41.3 | 51.1 | 31.1 | 31.4 | 15.8 | 31.7 | 39.7 | 35.0 |
| F & C to B | [18] | 34.5 | 30.4 | 44.2 | 21.2 | 19.0 | 0.0 | 9.2 | 22.8 | 22.7 |
| | DGFR-CNN (Ours) | 44.8 | 30.4 | 59.4 | 10.8 | 14.4 | 0.1 | 22.9 | 16.7 | 24.9 |

- [3] Wei Liu, Dragomir Anguelov, Dumitru Erhan, Christian Szegedy, Scott Reed, Cheng-Yang Fu, and Alexander C Berg. SSD: Single shot multibox detector. In *European Conference on Computer Vision*, pages 21–37. Springer, 2016.
- [4] Shaoqing Ren, Kaiming He, Ross Girshick, and Jian Sun. Faster R-CNN: Towards real-time object detection with region proposal networks. *Advances in neural information processing systems*, 28:91–99, 2015.
- [5] Tsung-Yi Lin, Piotr Dollár, Ross Girshick, Kaiming He, Bharath Hariharan, and Serge Belongie. Feature pyramid networks for object detection. In *Proceedings of the IEEE Conference on Computer Vision and Pattern Recognition*, pages 2117–2125, 2017.
- [6] Jifeng Dai, Yi Li, Kaiming He, and Jian Sun. R-FCN: Object detection via region-based fully convolutional networks. In D. Lee, M. Sugiyama, U. Luxburg, I. Guyon, and R. Garnett, editors, *Advances in Neural Information Processing Systems*, volume 29. Curran Associates, Inc., 2016.
- [7] Mark Everingham, Luc Van Gool, Christopher KI Williams, John Winn, and Andrew Zisserman. The Pascal visual object classes (VOC) challenge. *International Journal of Computer Vision*, 88(2):303–338, 2010.
- [8] Tsung-Yi Lin, Michael Maire, Serge Belongie, James Hays, Pietro Perona, Deva Ramanan, Piotr Dollár, and C Lawrence Zitnick. Microsoft COCO: Common objects in context. In *European Conference on Computer Vision*, pages 740–755. Springer, 2014.
- [9] Benjamin Recht, Rebecca Roelofs, Ludwig Schmidt, and Vaishaal Shankar. Do imagenet classifiers generalize to imagenet? In *International Conference on Machine Learning*, pages 5389–5400. PMLR, 2019.
- [10] Dan Hendrycks and Thomas Dietterich. Benchmarking neural network robustness to common corruptions and perturbations. *arXiv preprint arXiv:1903.12261*, 2019.
- [11] Kaiyang Zhou, Ziwei Liu, Yu Qiao, Tao Xiang, and Chen Change Loy. Domain generalization: A survey. *arXiv preprint arXiv:2103.02503*, 2021.
- [12] Pang Wei Koh, Shiori Sagawa, Sang Michael Xie, Marvin Zhang, Akshay Balsubramani, Weihua Hu, Michihiro Yasunaga, Richard Lanus Phillips, Irena Gao, Tony Lee, et al. Wilds: A benchmark of in-the-wild distribution shifts. In *International Conference on Machine Learning*, pages 5637–5664. PMLR, 2021.
- [13] Jose G Moreno-Torres, Troy Raeder, Rocío Alaiz-Rodríguez, Nitesh V Chawla, and Francisco Herrera. A unifying view on dataset shift in classification. *Pattern recognition*, 45(1):521–530, 2012.

- [14] Hong Liu, Pinhao Song, and Runwei Ding. Towards domain generalization in underwater object detection. In *2020 IEEE International Conference on Image Processing (ICIP)*, pages 1971–1975. IEEE, 2020.
- [15] Yuhua Chen, Wen Li, Christos Sakaridis, Dengxin Dai, and Luc Van Gool. Domain adaptive Faster R-CNN for object detection in the wild. In *Proceedings of the IEEE Conference on Computer Vision and Pattern Recognition*, pages 3339–3348, 2018.
- [16] Karthik Seemakurthy, Petra Bosilj, Erchan Aptoula, and Charles Fox. Domain generalised fully convolutional one stage detection. In *International Conference on Robotics and Automation (ICRA)*. IEEE, 2023.
- [17] Karthik Seemakurthy, Charles Fox, Erchan Aptoula, and Petra Bosilj. Domain generalised faster r-cnn. In *Thirty-Seventh AAAI Conference on Artificial Intelligence*, 2023.
- [18] Chuang Lin, Zehuan Yuan, Sicheng Zhao, Peize Sun, Changhu Wang, and Jianfei Cai. Domain-invariant disentangled network for generalizable object detection. In *Proceedings of the IEEE/CVF International Conference on Computer Vision*, pages 8771–8780, 2021.
- [19] Yang Chen, Pinhao Song, Hong Liu, Linhui Dai, Xiaochuan Zhang, Runwei Ding, and Shengquan Li. Achieving domain generalization for underwater object detection by domain mixup and contrastive learning. *Neurocomput.*, 528(C):20–34, apr 2023. doi: 10.1016/j.neucom.2023.01.053.
- [20] Navneet Dalal and Bill Triggs. Histograms of oriented gradients for human detection. In *2005 IEEE Computer Society Conference on Computer Vision and Pattern Recognition (CVPR'05)*, volume 1, pages 886–893. Ieee, 2005.
- [21] Pedro F Felzenszwalb, Ross B Girshick, David McAllester, and Deva Ramanan. Object detection with discriminatively trained part-based models. *IEEE Transactions on Pattern Analysis and Machine Intelligence*, 32(9): 1627–1645, 2009.
- [22] Paul Viola and Michael Jones. Rapid object detection using a boosted cascade of simple features. In *Proceedings of the 2001 IEEE Computer Society Conference on Computer Vision and Pattern Recognition. CVPR 2001*, volume 1, pages I–I. Ieee, 2001.
- [23] Yann LeCun, Léon Bottou, Yoshua Bengio, and Patrick Haffner. Gradient-based learning applied to document recognition. *Proceedings of the IEEE*, 86(11):2278–2324, 1998.
- [24] Alex Krizhevsky, Ilya Sutskever, and Geoffrey E Hinton. Imagenet classification with deep convolutional neural networks. *Advances in neural information processing systems*, 25:1097–1105, 2012.
- [25] Joseph Redmon and Ali Farhadi. Yolov3: An incremental improvement. *arXiv preprint arXiv:1804.02767*, 2018.
- [26] Joseph Redmon, Santosh Divvala, Ross Girshick, and Ali Farhadi. You only look once: Unified, real-time object detection. In *Proceedings of the IEEE Conference on Computer Vision and Pattern Recognition*, pages 779–788, 2016.
- [27] Zhi Tian, Chunhua Shen, Hao Chen, and Tong He. Fcos: Fully convolutional one-stage object detection. In *Proceedings of the IEEE/CVF international conference on computer vision*, pages 9627–9636, 2019.
- [28] Nicolas Carion, Francisco Massa, Gabriel Synnaeve, Nicolas Usunier, Alexander Kirillov, and Sergey Zagoruyko. End-to-end object detection with transformers. In *European conference on computer vision*, pages 213–229. Springer, 2020.
- [29] Liqiang He and Sinisa Todorovic. Destr: Object detection with split transformer. In *Proceedings of the IEEE/CVF Conference on Computer Vision and Pattern Recognition (CVPR)*, pages 9377–9386, June 2022.
- [30] Gongjie Zhang, Zhipeng Luo, Zichen Tian, Jingyi Zhang, Xiaoqin Zhang, and Shijian Lu. Towards efficient use of multi-scale features in transformer-based object detectors. In *2023 IEEE/CVF Conference on Computer Vision and Pattern Recognition (CVPR)*, pages 6206–6216, 2023.
- [31] Zhou Huang, Hang Dai, Tian-Zhu Xiang, Shuo Wang, Huai-Xin Chen, Jie Qin, and Huan Xiong. Feature shrinkage pyramid for camouflaged object detection with transformers. In *2023 IEEE/CVF Conference on Computer Vision and Pattern Recognition (CVPR)*, pages 5557–5566, 2023.

- [32] Ross Girshick, Jeff Donahue, Trevor Darrell, and Jitendra Malik. Rich feature hierarchies for accurate object detection and semantic segmentation. In *Proceedings of the IEEE Conference on Computer Vision and Pattern Recognition*, pages 580–587, 2014.
- [33] Ross Girshick. Fast R-CNN. In *Proceedings of the IEEE International Conference on Computer Vision*, pages 1440–1448, 2015.
- [34] Sinno Jialin Pan and Qiang Yang. A survey on transfer learning. *IEEE Transactions on knowledge and data engineering*, 22(10):1345–1359, 2010.
- [35] Jia Deng, Wei Dong, Richard Socher, Li-Jia Li, Kai Li, and Li Fei-Fei. Imagenet: A large-scale hierarchical image database. In *2009 IEEE conference on computer vision and pattern recognition*, pages 248–255. Ieee, 2009.
- [36] Fuzhen Zhuang, Zhiyuan Qi, Keyu Duan, Dongbo Xi, Yongchun Zhu, Hengshu Zhu, Hui Xiong, and Qing He. A comprehensive survey on transfer learning. *Proceedings of the IEEE*, 109(1):43–76, 2020.
- [37] Petra Bosilj, Erchan Aptoula, Tom Duckett, and Grzegorz Cielniak. Transfer learning between crop types for semantic segmentation of crops versus weeds in precision agriculture. *Journal of Field Robotics*, 37(1):7–19, 2020.
- [38] Mostafa Mehdipour Ghazi, Berrin Yanikoglu, and Erchan Aptoula. Plant identification using deep neural networks via optimization of transfer learning parameters. *Neurocomputing*, 235:228–235, 2017.
- [39] Shuteng Niu, Yongxin Liu, Jian Wang, and Houbing Song. A decade survey of transfer learning (2010–2020). *IEEE Transactions on Artificial Intelligence*, 1(2):151–166, 2020.
- [40] Kaixin Wang, Jun Hao Liew, Yingtian Zou, Daquan Zhou, and Jiashi Feng. Panet: Few-shot image semantic segmentation with prototype alignment. In *proceedings of the IEEE/CVF international conference on computer vision*, pages 9197–9206, 2019.
- [41] Longlong Jing and Yingli Tian. Self-supervised visual feature learning with deep neural networks: A survey. *IEEE transactions on pattern analysis and machine intelligence*, 43(11):4037–4058, 2020.
- [42] Mehdi Noroozi and Paolo Favaro. Unsupervised learning of visual representations by solving jigsaw puzzles. In *European conference on computer vision*, pages 69–84. Springer, 2016.
- [43] Julia Hindel, Nikhil Gosala, Kevin Bregler, and Abhinav Valada. Inod: Injected noise discriminator for self-supervised representation learning in agricultural fields. *arXiv preprint arXiv:2303.18101*, 2023.
- [44] Melike Ilteralp, Sema Ariman, and Erchan Aptoula. A deep multitask semisupervised learning approach for chlorophyll-a retrieval from remote sensing images. *Remote Sensing*, 14(1):18, 2021.
- [45] Zahid Ullah, Muhammad Usman, Siddique Latif, Asifullah Khan, and Jeonghwan Gwak. Ssm-d-unet: semi-supervised multi-task decoders network for diabetic retinopathy segmentation. *Scientific Reports*, 13(1):9087, 2023.
- [46] Wei-Hong Li, Xialei Liu, and Hakan Bilen. Learning multiple dense prediction tasks from partially annotated data. In *Proceedings of the IEEE/CVF Conference on Computer Vision and Pattern Recognition*, pages 18879–18889, 2022.
- [47] Yongxin Yang and Timothy M Hospedales. Deep multi-task representation learning: A tensor factorisation approach. In *International Conference on Learning Representations*, 2016.
- [48] Shujun Wang, Lequan Yu, Caizi Li, Chi-Wing Fu, and Pheng-Ann Heng. Learning from extrinsic and intrinsic supervisions for domain generalization. In *European Conference on Computer Vision*, pages 159–176. Springer, 2020.
- [49] Josh Tobin, Rachel Fong, Alex Ray, Jonas Schneider, Wojciech Zaremba, and Pieter Abbeel. Domain randomization for transferring deep neural networks from simulation to the real world. In *2017 IEEE/RSJ International Conference on Intelligent Robots and Systems (IROS)*, pages 23–30. IEEE, 2017.
- [50] Xiangyu Yue, Yang Zhang, Sicheng Zhao, Alberto Sangiovanni-Vincentelli, Kurt Keutzer, and Boqing Gong. Domain randomization and pyramid consistency: Simulation-to-real generalization without accessing target domain data. In *Proceedings of the IEEE/CVF International Conference on Computer Vision*, pages 2100–2110, 2019.

- [51] Kate Saenko, Brian Kulis, Mario Fritz, and Trevor Darrell. Adapting visual category models to new domains. In *European Conference on Computer Vision*, pages 213–226. Springer, 2010.
- [52] Gilles Blanchard, Gyemin Lee, and Clayton Scott. Generalizing from several related classification tasks to a new unlabeled sample. *Advances in neural information processing systems*, 24:2178–2186, 2011.
- [53] Krikamol Muandet, David Balduzzi, and Bernhard Schölkopf. Domain generalization via invariant feature representation. In *International Conference on Machine Learning*, pages 10–18. PMLR, 2013.
- [54] Aditya Khosla, Tinghui Zhou, Tomasz Malisiewicz, Alexei A Efros, and Antonio Torralba. Undoing the damage of dataset bias. In *European Conference on Computer Vision*, pages 158–171. Springer, 2012.
- [55] Zheng Xu, Wen Li, Li Niu, and Dong Xu. Exploiting low-rank structure from latent domains for domain generalization. In *European Conference on Computer Vision*, pages 628–643. Springer, 2014.
- [56] Chen Fang, Ye Xu, and Daniel N Rockmore. Unbiased metric learning: On the utilization of multiple datasets and web images for softening bias. In *Proceedings of the IEEE International Conference on Computer Vision*, pages 1657–1664, 2013.
- [57] Muhammad Ghifary, W Bastiaan Kleijn, Mengjie Zhang, and David Balduzzi. Domain generalization for object recognition with multi-task autoencoders. In *Proceedings of the IEEE International Conference on Vision*, pages 2551–2559, 2015.
- [58] Da Li, Yongxin Yang, Yi-Zhe Song, and Timothy M Hospedales. Deeper, broader and artier domain generalization. In *Proceedings of the IEEE International Conference on Computer Vision*, pages 5542–5550, 2017.
- [59] Da Li, Yongxin Yang, Yi-Zhe Song, and Timothy M Hospedales. Learning to generalize: Meta-learning for domain generalization. In *Thirty-Second AAAI Conference on Artificial Intelligence*, 2018.
- [60] Shiv Shankar, Vihari Piratla, Soumen Chakrabarti, Siddhartha Chaudhuri, Preethi Jyothi, and Sunita Sarawagi. Generalizing across domains via cross-gradient training. In *ICLR*, 2018.
- [61] Da Li, Jianshu Zhang, Yongxin Yang, Cong Liu, Yi-Zhe Song, and Timothy M Hospedales. Episodic training for domain generalization. In *Proceedings of the IEEE/CVF International Conference on Computer Vision*, pages 1446–1455, 2019.
- [62] Yaroslav Ganin, Evgeniya Ustinova, Hana Ajakan, Pascal Germain, Hugo Larochelle, François Laviolette, Mario Marchand, and Victor Lempitsky. Domain-adversarial training of neural networks. *The journal of machine learning research*, 17(1):2096–2030, 2016.
- [63] Ya Li, Xinmei Tian, Mingming Gong, Yajing Liu, Tongliang Liu, Kun Zhang, and Dacheng Tao. Deep domain generalization via conditional invariant adversarial networks. In *Proceedings of the European Conference on Computer Vision (ECCV)*, pages 624–639, 2018.
- [64] M. Ghifary, D. Balduzzi, W.B. Kleijn, and M. Zhang. Scatter component analysis: A unified framework for domain adaptation and domain generalization. *IEEE transactions on pattern analysis and machine intelligence*, 39(7):1414–1430, 2016.
- [65] D. Mahajan, S. Tople, and A. Sharma. Domain generalization using causal matching. In *Proceedings of ICML*, pages 7313–7324, 2021.
- [66] H. Li, Y. Wang, R. Wan, S. Wang, T-Q. Li, and A. Kot. Domain generalization for medical imaging classification with linear-dependency regularization. *Advances in neural information processing systems*, 33:3118–3129, 2020.
- [67] Haoliang Li, Sinno Jialin Pan, Shiqi Wang, and Alex C Kot. Domain generalization with adversarial feature learning. In *Proceedings of the IEEE Conference on Computer Vision and Pattern Recognition*, pages 5400–5409, 2018.
- [68] Maximilian Ilse, Jakub M Tomczak, Christos Louizos, and Max Welling. Diva: Domain invariant variational autoencoders. In *Medical Imaging with Deep Learning*, pages 322–348. PMLR, 2020.
- [69] Chelsea Finn, Pieter Abbeel, and Sergey Levine. Model-agnostic meta-learning for fast adaptation of deep networks. In *International conference on machine learning*, pages 1126–1135. PMLR, 2017.

- [70] Qi Dou, Daniel Coelho de Castro, Konstantinos Kamnitsas, and Ben Glocker. Domain generalization via model-agnostic learning of semantic features. *Advances in neural information processing systems*, 32, 2019.
- [71] Yingjun Du, Xiantong Zhen, Ling Shao, and Cees GM Snoek. Metanorm: Learning to normalize few-shot batches across domains. In *International Conference on Learning Representations*, 2020.
- [72] Yuge Shi, Jeffrey Seely, Philip Torr, Siddharth N, Awni Hannun, Nicolas Usunier, and Gabriel Synnaeve. Gradient matching for domain generalization. In *International Conference on Learning Representations*, 2022. URL <https://openreview.net/forum?id=vDwBW49Hm0>.
- [73] Kaiyang Zhou, Yongxin Yang, Timothy Hospedales, and Tao Xiang. Learning to generate novel domains for domain generalization. In *Computer Vision—ECCV 2020: 16th European Conference, Glasgow, UK, August 23–28, 2020, Proceedings, Part XVI 16*, pages 561–578. Springer, 2020.
- [74] Jifei Song, Yongxin Yang, Yi-Zhe Song, Tao Xiang, and Timothy M Hospedales. Generalizable person re-identification by domain-invariant mapping network. In *Proceedings of the IEEE/CVF conference on Computer Vision and Pattern Recognition*, pages 719–728, 2019.
- [75] Guoqing Wang, Hu Han, Shiguang Shan, and Xilin Chen. Cross-domain face presentation attack detection via multi-domain disentangled representation learning. In *Proceedings of the IEEE/CVF conference on computer vision and pattern recognition*, pages 6678–6687, 2020.
- [76] Yunpei Jia, Jie Zhang, Shiguang Shan, and Xilin Chen. Single-side domain generalization for face anti-spoofing. In *Proceedings of the IEEE/CVF Conference on Computer Vision and Pattern Recognition*, pages 8484–8493, 2020.
- [77] Shanshan Zhao, Mingming Gong, Tongliang Liu, Huan Fu, and Dacheng Tao. Domain generalization via entropy regularization. *Advances in Neural Information Processing Systems*, 33, 2020.
- [78] Bernhard Schölkopf, Dominik Janzing, Jonas Peters, Eleni Sgouritsa, Kun Zhang, and Joris Mooij. On causal and anticausal learning. *arXiv preprint arXiv:1206.6471*, 2012.
- [79] Dominik Janzing and Bernhard Schölkopf. Causal inference using the algorithmic markov condition. *IEEE Transactions on Information Theory*, 56(10):5168–5194, 2010.
- [80] Shoubo Hu, Kun Zhang, Zhitang Chen, and Laiwan Chan. Domain generalization via multidomain discriminant analysis. In *Uncertainty in Artificial Intelligence*, pages 292–302. PMLR, 2020.
- [81] Martin Arjovsky, Léon Bottou, Ishaan Gulrajani, and David Lopez-Paz. Invariant risk minimization. *arXiv preprint arXiv:1907.02893*, 2019.
- [82] Toshihiko Matsuura and Tatsuya Harada. Domain generalization using a mixture of multiple latent domains. In *Proceedings of the AAAI Conference on Artificial Intelligence*, volume 34, pages 11749–11756, 2020.
- [83] Ian J Goodfellow, Jean Pouget-Abadie, Mehdi Mirza, Bing Xu, David Warde-Farley, Sherjil Ozair, Aaron Courville, and Yoshua Bengio. Generative adversarial networks. *arXiv preprint arXiv:1406.2661*, 2014.
- [84] Dominik Maria Endres and Johannes E Schindelin. A new metric for probability distributions. *IEEE Transactions on Information theory*, 49(7):1858–1860, 2003.
- [85] Mingming Gong, Yanwu Xu, Chunyuan Li, Kun Zhang, and Kayhan Batmanghelich. Twin auxiliary classifiers GAN. *Advances in neural information processing systems*, 32:1328, 2019.
- [86] Marius Cordts, Mohamed Omran, Sebastian Ramos, Timo Rehfeld, Markus Enzweiler, Rodrigo Benenson, Uwe Franke, Stefan Roth, and Bernt Schiele. The Cityscapes dataset for semantic urban scene understanding. In *Proceedings of the IEEE Conference on Computer Cision and Pattern Recognition*, pages 3213–3223, 2016.
- [87] Christos Sakaridis, Dengxin Dai, and Luc Van Gool. Semantic foggy scene understanding with synthetic data. *International Journal of Computer Vision*, 126(9):973–992, Sep 2018.
- [88] Fisher Yu, Haofeng Chen, Xin Wang, Wenqi Xian, Yingying Chen, Fangchen Liu, Vashisht Madhavan, and Trevor Darrell. Bdd100k: A diverse driving dataset for heterogeneous multitask learning. In *Proceedings of the IEEE/CVF conference on computer vision and pattern recognition*, pages 2636–2645, 2020.

- [89] Christos Sakaridis, Dengxin Dai, and Luc Van Gool. ACDC: The adverse conditions dataset with correspondences for semantic driving scene understanding. In *Proceedings of the IEEE/CVF International Conference on Computer Vision (ICCV)*, October 2021.
- [90] Girish Varma, Anbumani Subramanian, Anoop Namboodiri, Manmohan Chandraker, and CV Jawahar. Idd: A dataset for exploring problems of autonomous navigation in unconstrained environments. In *2019 IEEE Winter Conference on Applications of Computer Vision (WACV)*, pages 1743–1751. IEEE, 2019.
- [91] Etienne David, Mario Serouart, Daniel Smith, Simon Madec, Kaaviya Velumani, Shouyang Liu, Xu Wang, Francisco Pinto, Shahameh Shafiee, Izzat SA Tahir, et al. Global wheat head detection 2021: an improved dataset for benchmarking wheat head detection methods. *Plant Phenomics*, 2021, 2021.